For submission to "PLOS ONE

Our file: Reid2021-Vf"

Regulation of skeletal muscle metabolism and contraction performance via teneurin-latrophilin action.

Andrea L. Reid[1], David W. Hogg[1], Thomas L. Dodsworth[1], Yani Chen[1], Ross M. Reid[2], Mei Xu[1], Mia Husic[1], Peggy R. Biga[2], Andrew Slee[3], Leslie T. Buck[1] Dalia Barsyte-Lovejoy[4], Marius Locke[5], David A. Lovejoy[1]*

1. Department of Cell and Systems Biology, University of Toronto, Toronto, ON Canada, 2. Department of Biology, University of Alabama, Birmingham AL USA, 3. Protagenic Therapeutics, Inc, Lexington MA USA, 4. Structural Genomics Consortium, University of Toronto, Toronto, ON Canada 5. Department of Kinesiology, University of Toronto, Toronto, ON Canada.

***Corresponding Author:** David A. Lovejoy, Ph.D
Department of Cell and Systems Biology
University of Toronto,
Toronto, Ontario
M5G 3G5, Canada
Email: david.lovejoy@utoronto.ca
Tel: +1 (647) 999 2977

Number of Words: 13,243

Number of Figures: 11

Number of Tables: 3

Number of References: 72

Keywords: TCAP, GPCR, peptides, diabetes, calcium, CRISPR, siRNA, mitochondria

Abstract

Skeletal muscle regulation is responsible for voluntary muscular movement in vertebrates. The genes of two essential proteins, teneurins and latrophilins (LPHN), evolving in ancestors of multicellular animals, form a ligand-receptor pair, and are now shown to be required for skeletal muscle function. Teneurins possess a bioactive peptide, termed the teneurin C-terminal associated peptide (TCAP) that interacts with the LPHNs to regulate skeletal muscle contractility strength and fatigue by an insulin-independent glucose importation mechanism. CRISPR-based knockouts and siRNA-associated knockdowns of LPHN-1 and-3 shows that TCAP stimulates an LPHN-mediated cytosolic Ca^{2+} signal transduction cascade to increase energy metabolism and enhance skeletal muscle function via increases in type-1 oxidative fiber formation and reduce the fatigue response. Thus, the teneurin/TCAP-LPHN system is presented as a novel mechanism likely to regulate the energy requirements and performance of skeletal muscle.

Introduction

Skeletal muscle is critical for all voluntary behaviours and is derived from the earliest contractile proteins present in the ancestral single-celled heterotrophs. Enhanced contractile strength and efficient energy metabolism among these primitive skeletal muscle cells were critical for both locomotion and feeding [1,2]. Because of these integrated requirements for the evolutionary success of early metazoans, we have postulated that essential intercellular signaling systems originating phylogenetically early, conferred a selective advantage upon these basal heterotrophs by linking sensory and motor functions with cell metabolism [3]. Numerous studies have indicated that the teneurins and their receptors, the latrophilins (LPHN) are part of an ancient regulatory system that modulates cell adhesion and metabolism. The introduction of the teneurin and LPHN genes into multicellular animals occurred via lateral gene transfer from prokaryotes into a single-celled ancestor of metazoans [4-9]. Thus, the teneurins and LPHNs were evolutionarily poised to play a seminal role in the development and coordination of cell-to-cell communication, adhesion and metabolic activities.

Teneurins are essential for development and maintenance of the central nervous system (CNS) [10-18]. Comprising a family of four paralogous proteins in vertebrates, the teneurins possess several functional domains that confer specialized actions on their extracellular and intracellular regions [19-21]. As type-II proteins, their carboxyl terminus is displaced extracellularly. The most distal region contains a β-barrel structure unique to metazoans, but is similar to that found in prokaryotic Tc-toxins [9,14,22-25]. Associated with this structure lies an extended amino-acid chain termed the ‘teneurin C-terminal associated peptide’ (TCAP) [22-24]. The TCAPs possess primary structure similarity to the Secretin superfamily of peptides that include, not only secretin paralogues such as vasoactive intestinal peptide (VIP), growth hormone-releasing hormone

(GHRH), glucagon and pituitary adenylate cyclase activating peptide (PACAP), but also the calcitonin and corticotropin-releasing factor (CRF) families. One of the distinguishing aspects of this peptide superfamily are their roles in the coordination of sensory, motor and energy metabolism [3,26,27].

The LPHNs are G-protein-coupled receptors (GPCR) belonging to the Adhesion GPCR family (ADGRL) and are cognate receptors of the teneurins in vertebrates [28-30]. LPHNs have three distinct paralogous forms (LPHN1-3) and can bind to the C-terminal region of the teneurins, which include the TCAP region. For example, Teneurin-2 and LPHN-1 binds with nanomolar affinity at the lectin-domain of LPHN-1[31]. A splice variant of C-terminal domain of teneurin-2, also termed 'LPHN1-associated synaptic surface organizer' (Lasso), binds to LPHN with, likewise, high affinity in neurons. Moreover, transgenic over-expression of both TCAP-1 and the hormone-binding domain (HBD) of LPHN-1 results in co-precipitation of both transgenic proteins indicating an interaction between TCAP-1 and LPHN-1 [32]. Recent structural studies of the teneurins indicate that the TCAP region may be auto-catalytically cleaved from the teneurins after interaction with the LPHNs [14,22], or could be the result of a distinct teneurin splice variant resulting in the mRNA expression of the terminal exon that includes the TCAP sequence [33,34].

Regardless of the mechanism of TCAP release, the expected TCAP mature peptide, based on its genomic sequence, has distinct biological properties. Synthetic TCAP-1 regulates cytoskeletal elements and energy metabolism in neurons critical for neuroplastic modulation in the central nervous system (CNS). In rats, TCAP-1 modifies dendritic arborization and spine density in the hippocampus [35,36], findings that were corroborated in primary cultures of rat embryonic hippocampal tissues that exhibited increased filopodia, neurite and axon development [33,37,38]. Thus, these actions indicate a role of TCAP-1 in CNS energy metabolism. Moreover, subcutaneous

91 administration of TCAP-1 into rats increases brain glucose uptake as assessed by functional
92 positron emission tomography (fPET). These observations were corroborated by the expected
93 decreased serum glucose and insulin levels in rats, and in cell culture studies showing that TCAP-1
94 stimulates glucose uptake by increased glucose transporter transit to the membrane and
95 subsequently increases in ATP turnover providing increased energy for the neurons [39].

96 However, given the evolutionary history of the teneurins, it is plausible that the teneurins, LPHNs,
97 and TCAP could also play a role in the regulation of skeletal muscle. Skeletal muscle is one of the
98 most important sites of glucose metabolism and is responsible for 40% of glucose-associated
99 energy requirements [39] and 80% of glucose uptake under insulin-stimulated conditions [40].
100 Muscle function and metabolism are intrinsically linked, as evidenced by metabolic syndromes
101 that result in poor muscle function and degradation. A key example of this is demonstrated in
102 patients with type-II diabetes where patients have reduced skeletal muscle function in the grip
103 force test compared to non-diabetic patients [41,42].

104 Based on these previous findings, we investigated the role of TCAP-1 on skeletal muscle function
105 for the first time. We demonstrate that skeletal muscle possesses the critical elements of teneurin-
106 LPHN interaction, and show that TCAP-1 regulates skeletal muscle contractile kinetics *in vivo* in
107 rats. These studies are supplemented by *in vitro* studies, using the mouse skeletal cell line, C2C12,
108 to show that TCAP regulates intracellular skeletal Ca^{2+} flux similar to that shown in neurons [3,39].
109 Moreover, like neurons, the TCAP-mediated Ca^{+2} response leads to increased glucose metabolism
110 and mitochondrial activation, but results in skeletal muscle fiber regulation. We posit that the
111 teneurin-LPHN interaction is essential for skeletal muscle physiology and regulates skeletal
112 muscle performance.

Materials and Methods

Peptide Synthesis and Solubilization

Both peptides; rat/mouse TCAP-1 and scrambled TCAP-1 (Fig. 1), were synthesized commercially by AmbioPharm, Inc. and prepared as an acetylated salt at 95% purity. Peptides were solubilized in saline after alkalization as previously described [37] then diluted into the required media for *in vitro* or *in vivo* studies (see below). The primary structure of all four rat and mouse TCAPs are identical to each other (Fig.1A) and possess a 73-83% sequence identity among the overall sequences, although most of these changes reflect homologous and conservative substitutions. For this reason, TCAP-1 was used in both rat and mouse preparations. Synthetic rat/mouse TCAP was prepared with an initial N-terminal pyroglutamic acid to inhibit N-terminal-directed peptidases, and a C-terminal amidated-residue as expected based on the genomic sequence [24,37]. As a control peptide, we have utilized a scrambled (sc) amino acid sequence version of rat/mouse TCAP-1 where each residue, with the exception of the initial pyroglutamyl residue (pE), was randomized in its placement within the peptide (Fig. 1B). This sc-TCAP-1 has been used in previous studies to establish an additional level of controls to ensure that TCAP-1 is not affecting non-specific (e.g. oligopeptide transporters; non-target receptors) actions. The vehicle included sc-TCAP solubilized in 0.9% saline or cell culture medium, unless otherwise stated.

Figure 1. Primary structures of rat and mouse TCAP peptides. A. Comparison of the amino acid sequences of mouse and rat TCAPs. **B**. Primary structure of the peptides used in this study. Grey boxed regions indicates regions of identity relative to the rat/mouse TCAP isoforms.

Animals

Male adult Sprague-Dawley (SD) rats (Charles River, Canada) were used for the short-term and long-term muscle function studies. The metabolic and endocrine studies of TCAP-1 on rats were approved by the University of Toronto Animal Care Committee (UACC) under the auspices of the Canadian Council of Animal Care. Male adult Wistar rats (~250 g) (Charles River, USA) were used for the functional positron emission tomography (fPET) studies performed by Molecular Imaging, Inc. (Ann Arbor, MI, USA) and approved by the American Association of Animal Laboratory Care (Hogg et al., 2019). In both sets of studies, animals were weighed weekly and monitored for any signs of distress or illness (e.g. loss of hair, extreme weight loss, abnormal behaviours). However, no animals showed overt indications of stress and all were utilized for these studies.

In Vivo Studies

The short-term application of TCAP-1 utilized 16 male adult SD rats (250g) that were acclimated for 1 week (w) on a 12:12 light-dark (LD) cycle. For 5 days (d) daily, the animals were treated with either vehicle or TCAP-1 (10 nmoles/kg) by subcutaneous (SC) injection in the intrascapular region. Animals were tested for muscle function by electrical muscle stimulation (see below) 3d after the last treatment. Animals were immediately euthanized afterward. For the long-term study, 20 adult male SD rats (350g), acclimated for 1w on a 12:12 LD cycle and were treated with either vehicle or intrascapular TCAP-1 (SC; 25 nmoles/kg) for 3 months (1 injection/week). Muscle

function by electrical muscle stimulation was tested 2w after the last treatment. Animals were immediately euthanized after electrical muscle stimulation studies (see below).

PCR Expression of teneurin and LPHN

RNA was extracted from tibialis anterior (TA) muscles using TRIzol (Thermo Scientific, Waltham, MA, USA) following the manufacturer's instructions. The PCR reaction mix included 5 µL cDNA, 2 µL forward primer and 2 µL reverse primer (Invitrogen; Table 1), 14.2 µL water (Sigma, Oakville, ON), 3 µL 10x Taq Buffer with KCl (Thermo Scientific), 1.8 µL $MgCl_2$ (Thermo Scientific), 1 µL deoxynucleotide Solution Mix and 0.5 µL Taq DNA Polymerase (New England Biolabs). The reactions were incubated in an Eppendorf Mastercycler Gradient Thermal Cycler for 7m at 95°C; followed by 35 cycles of 60s at 95°C, 90s at 67°C, and 35s at 72°C; and then held at 4°C. cDNA samples were resolved on a 3% agarose gel at 100 V for 1.5h and visualized using a Bio-Rad ChemiDoc MP System with 0.5s exposure.

Table 1. Primers used for in vitro and in vitro RT-PCR analyses. Forward and reverse primer pairs for the four teneurins, TCAPs, three ADGRLs, and β-actin control are indicated.

Gene	Forward Primer (5'-3')	Reverse Primer (5'-3')	Expected band size
Teneurin-1	CACAGTCAGCGGCGTTACATCTTTGAG	GAATCCGTCATGCATCAGGTGTATTGT	342 bp
Teneurin-2	ATCCTGAACTCGCCGTCCTCCTTA	CTCCAGGTTCTGAGTGGACACGGC	405 bp
Teneurin-3	GTGAGTACCGTTGATGTCAAAGATG	AGTGGAATACCCGGTGGGGAAGCAC	427 bp
Teneurin-4	ATCGACCAATTCCTGCTGAGCAAG	CCAGAGAGGCATCCCGGTAGAGTC	567 bp
TCAP-1	ACGTCAGTGTTGAATGGGAGGACTA	CCTCCTGCCTATTTCACTCTGTCTCAT	351 bp
TCAP-2	GACAAGATGCACTACAGCATCGAG	CCATCTCATTCTGTCTTAAGAACTGG	496 bp
TCAP-3	CAACAACGCCTTCTACCTGGAGAAC	CGATCTCACTTTGTCGCAAGAACT	506 bp
TCAP-4	TTTGCCTCCAGTGGTTCCATCTT	TGGATATTGTTGGCGCTGTCTGAC	602 bp
ADGRL1	AGCCAGAGGACTTGACTCA	TTCTAGGCCTCAGAGCTACAT	249 bp
ADGRL2	TGGAGCAAAAAGTC	TTCAAAACAGC	203 bp
ADGRL3	TGAGCAACTGTGTGCAAATT	TAACCACCAGCCACACCAT	327 bp
β-actin	CAGCCATGTACGTAGCCATCCA	ATGTCACGCACGATTTCCCTCT	247 bp

Histological Studies

TA muscle was excised then flash-frozen in liquid nitrogen cooled-isopentane. The tissue was cryo-sectioned at 10 μm at -20˚C and transferred to coverslides and fixed using ice-cold methanol. Following blocking for 1h with 10% normal goat serum (NGS: Cell Signaling, Inc.), the primary antibody (Table 2), diluted in 1% NGS, was added and incubated overnight (ON) at 4˚C. Subsequently, after 3 phosphate-buffered saline (PBS) washes, the secondary antibody was added and incubated for 1h at room temperature (RT) in the dark. Coverslips were attached, and the tissue imaged using confocal microscopy (Leica TCS-SP8) at 400x magnification. For fluorescence analyzes of protein expression, Image J software was used to measure arbitrary fluorescent units (AFU), where changes of AFU are proportional to protein expression changes. A total of 5 slides

were quantified with 8 regions of interest (ROI) investigated. ROI was defined as regions with multiple cell interactions free of artifacts.

Table 2. Primary and secondary antibodies used in western blot analyzes.

Name	Primary Antibody	Secondary Antibody	Expected band size
LPHN-1	Goat polyclonal IgG	Donkey anti-goat HRP-linked	130 kDa
LPHN-2	Goat polyclonal IgG	Donkey anti-goat HRP-linked	163 kDa
LPHN-3	Rabbit polyclonal IgG	Donkey anti-rabbit HRP-linked	162 kDa
SDH-A	Mouse monoclonal IgG	Rabbit anti-mouse HRP linked	70 kDa
β-actin	Mouse monoclonal IgG	Rabbit anti-mouse HRP linked	42kDa

Functional Positron Emission Tomography (fPET)

Male Wistar rats were treated with either vehicle or TCAP-1 (10 nmoles/kg) by intrascapular SC injection. 3d after treatment, 1 mCi of [^{18}F]-2-deoxyglucose (^{18}F-DG) radiotracer (IBA Molecular) was administered intravenously (IV) under anesthesia. fPET scans were performed using a Siemens Inveon microPET small animal PET scanner using the protocol as previously described [39]. Briefly, body temperature was maintained with a thermostat-regulated recirculating water-heated pad. Static emission data was acquired for 20m. The PET list mode data was converted to 2-dimensional (2D) sinograms, corrected for random coincidences, and normalized for scanner uniformity. The PET image analysis was performed using the Amira 5.5.0 analysis software package. For whole body ROIs (regions of high ^{18}F-DG uptake), a low threshold was set to

delineate specific signals in the whole body while eliminating background. The total PET counts were calculated from all voxels within the segmented volumes of interest. These images were then compiled into 3-dimensional (3D) projections, thus allowing for accurate analyzes of muscle tissue. Fluorescence of the mean pixel was calibrated to volume of muscle being analyzed (mean pixel fluorescence/mm^3).

NADH staining and analysis

TA muscles from the treated SD rats were cryo-sectioned at 10 µm thickness as described above. Cryo-sections were washed 2x with PBS, then 0.2% NBT solution in PBS (containing 0.1% NADH; Sigma, Oakville, ON) was added and incubated for 30m at 37°C. Slides were washed 2x in PBS before mounted, imaged at 100x magnification and analyzed on Image J software for pixel density, where darker pixels represent higher levels of NADH. Expression of NADH was analyzed based on a minimum of 100 fibres per tissue, with a minimum of 3-4 tissues analyzed for each group.

Muscle function and integrity testing by electrical muscle stimulation

The electrical muscle stimulation protocol was followed as described by Holwerda and Locke [43] with minor modifications. Briefly, animals were anesthetized with 5% isofluorane in 1L/min O_2, and subsequently positioned into the testing apparatus. A 25g needle was inserted through the soft tissue of the knee in order to ensure a stable position. The foot was placed on a lever attached to a servomotor and taped in position. Electrodes were placed below the skin but adjacent to the TA muscle. Dynamic Muscle Control (DMC; Version 5; Aurora Scientific) software was used for electrical stimulation and analyzes. The correct voltages for peak tetanic tension was established by increasing voltage by 1V increments until optimal tetanus twitch was achieved. The test began

with a single tetanus and single twitch protocol to establish the baseline followed by a 6-min fatigue protocol (8V, 200 Hz, 300 ms). After the termination of the protocol, tetanic and twitch tensions were recorded at 0, 1, and 5 mins. Animals were immediately euthanized after recovery measurements were recorded.

Quantitative Reverse-Transcription Polymerase Chain Reaction (qRT-PCR):

TA muscle mRNA and cDNA were prepared as previously described (see above). The cDNA from all samples was used to prepare pools to establish standard curves of each gene. The cDNA pool or cDNA samples were mixed with MasterMix containing SYBR select. The reactions were loaded in a 384-well PCR plate and run in a BioRAD qRT thermal cycler for 2m at 50°C, 7m at 95°C; followed by 39 cycles of 60s at 95°C, 90s at 67°C, and 35s at 72°C. Melting curves were established by a step-wise gradient from 60-90°C. The myosin heavy chain (MHC) isoforms, MHCI, MHCIIa, MHCIIx and MHCIIb were analyzed by real-time PCR using the mRNA and cDNA prepared above (see Table 3).

Table 3. Rat MHC isoforms and β-actin control primers used for qRT-PCR. Forward and reverse primer pairs are indicated for the four MHC isoforms.

Gene	Forward Primer (5'-3')	Reverse Primer (5'-3')
MHCI	GAATGGCAAGACGGTGACTGT	GGAAGCGTACCTCTCCTTGAGA
MHCIIa	ATGACAACTCCTCTCGCTTTG	TTAAGCTGGAAAGTGACCCGG
MHCIIb	GAACACGAAGCGTGTCATCCA	AGGTTTCGATATCTGCGGAGG
MHCIIx	CCAATGAGACTAAGACGCCTGG	GCTATCGATGAATTGTCCCTCG
β-actin	AGCCATGTACGTAGCCA	CTCTCAGCTGTGGTGGTGAA

In Vitro Studies

Culture and cDNA analyses of C2C12 cell line

The immortalized murine skeletal muscle cell line, C2C12, was used for all *in vitro* studies. Cells were maintained at 60-70% confluency with Dulbecco's Modified Eagle Medium (DMEM) supplemented with 20% fetal bovine serum (FBS) and a penicillin/streptomycin antibiotic combination (Invitrogen, Burlington, ON, Canada). To induce differentiation, the media was changed to DMEM supplemented with 10% horse serum (HS) with the penicillin/streptomycin antibiotic combination, and the cells were allowed to differentiate for 6d (media replaced every 24 hrs). For treatment, cells were serum-starved for 3h and then treated with either vehicle or TCAP-1 (100 nM). The identification of teneurin, TCAP and LPHN cDNAs in C2C12 cells was performed

with mRNA extracted from differentiated mouse C2C12 cells using the method described above using the primer sequences indicated in Table 1.

Live-cell calcium imaging in C2C12 myotubules

The C2C12 skeletal cells were grown and differentiated on poly-D-lysine-coated 25 mm round No. 1 glass coverslips (Warner Instruments, Hamden, CT, USA). Changes in intracellular Ca^{2+} were assessed using the membrane-permeable fluorescent indicator fluo-4, AM (Invitrogen, Burlington, ON, Canada). Cells were loaded with fluo-4 by incubating coverslips in DMEM containing 10 μM fluo-4 for 30m (37°C) followed by a 15m wash in Locke's Buffer (305-310 mOsmol at 22°C). In experiments assessing changes in intracellular Ca^{2+}, coverslips were placed in a flow-through bath chamber (RC-40HP, Warner Instruments, Hamden, CT, USA) of an inverted microscope (Axio Observer Z1, Zeiss, Toronto, ON, Canada) equipped with a 40× oil immersion objective. Cells were continuously bulk-perfused with Locke's buffer via a gravity drip perfusion system at a rate of 2–3 ml/min at RT. Changes in fluo-4 fluorescence were imaged using a green fluorescent protein (GFP) filter set (Semrock, Rochester, NY, USA) and a X-Cite 120 fluorescence illumination system (Excelitas Technologies, Mississauga, ON, Canada), controlled by Volocity 4.0 imaging software (Quorum Technologies Inc., Guelph, ON, Canada). Fluorescence emissions were detected with an Orca-ER Hamamatsu B/W CCD digital camera (Hamamatsu, Middlesex, NJ, USA). Fluo-4 was excited with a wavelength of 480 nm for 100ms every 3-5s and fluorescence emission was measured at wavelength of 516 nm.

330 **Caffeine stimulation experiments**

331 Caffeine action on the cells was used to establish that the cells were viable. Caffeine (4 mM;
332 Sigma-Aldrich, Oakville, ON) was applied to C2C12 myotubes to stimulate Ca^{2+} release from the
333 sarcoplasmic reticulum (SR). Cells were either pre-treated with TCAP-1 (100 nM) or vehicle for
334 1h before stimulation with caffeine. Using Velocity 4.0 imaging software, ROIs were taken from
335 cytosolic regions within the myotubules (n= 4 coverslips, 4-5 ROIs per coverslip).

336

337 **GLUT4 Immunocytochemical studies**

338 C2C12 cells were differentiated, as described above. After 3h of serum starvation, myotubules
339 were treated either with vehicle, TCAP-1 (100 nM) or insulin (100 nM) for 15 or 30m. Cells were
340 then fixed using 4% paraformaldehyde and subsequently blocked with 10% NGS for 1h at RT.
341 The GLUT4 primary antibody, diluted in 1% NGS, was added to the cells and incubated at 4°C
342 overnight (OT). Following 4 PBS washes, the secondary antibody (diluted in 1% NGS) was added
343 and incubated 1h at RT. The coverslips were mounted using DAPI-containing Vectashield. Slides
344 were imaged on a confocal microscope with a 40x oil objective. The images were analyzed using
345 Image J, where myotubules were selected as ROIs and were analyzed for red pixel intensity values,
346 representing GLUT4 levels, and normalized to area size (n= 3-4 coverslips per treatment, 7-8
347 myotubules per coverslip). For the IP3R inhibitor, 2-aminoethoxydiphenyl borate (2-APB; Sigma
348 Aldrich, Oakville, ON) experiments, 2-APB (100 µM) was applied for 4m before the start of
349 treatment with either sham (Locke's buffer) or TCAP-1 (100 nM), containing 2-APB for
350 continuous blocking of IP3R.

351

352

353 **Radioactive glucose uptake**

354 The ^{3}H-2-deoxyglucose uptake protocol was followed as previously described with minor
355 modifications [44,45]. At day-6 post-plating, C2C12 myotubules were washed 2x with Locke's
356 without serum and glucose. The culture was incubated in the Locke's buffer for 1h at 37°C
357 followed by exposure to 100 nM insulin, 100 nM TCAP-1, 100 nM SC-TCAP-1, or saline. ^{3}H-2-
358 deoxyglucose (0.5 μCi/ml) was added to the culture 5m before termination of treatment exposure.
359 Uptake of ^{3}H-2-deoxyglucose was stopped immediately after 5m with 3x washes of ice-cold 0.9%
360 saline solution. The cells were digested with 1 mL of 0.05 M NaOH at 0, 30, 45, and 60 min after
361 treatment. Radioactivity of the cell lysates were measured using a beta liquid scintillation counter
362 (Beckman Coulter), and recorded in counts per minute (CPM).

363

364 **Intracellular ATP and NADH assays**

365 ATP assays were conducted using Promega ATP Assay kits (Wisconsin, USA) following the
366 manufacturer's instructions. Briefly, C2C12 cells were seeded at 10,000 cells/well in 96-well
367 plates. The following day, cells were treated with either vehicle or TCAP-1 (100 nM) and lysed at
368 0, 15, 30 and 60m after treatment. Ultra-Glo recombinant luciferase (Promega, Wisconsin, USA)
369 was added to the media to determine ATP levels. Fluorescence from blank wells was subtracted
370 from all samples to account for background signal noise. As the fluorescence signal naturally
371 decays over the course of the experiment, TCAP-1-treated cells were compared relatively to the
372 vehicle-treated cells for each time point (n=8). For the resazurin NADH assay, the C2C12 cells
373 were seeded at 10,000 cells /well in 96-well plates. The resazurin assay was started the following
374 day by adding the resazurin solution (525 nM, Sigma) to all wells. Cells were treated with either
375 vehicle or TCAP-1 (100 nM). Fluorescent readings were measured every 5m over 1h, with

376 excitation at 530 nm and emission read at 590 nm. The measurements of blank wells not containing
377 cells were subtracted from all readings.
378
379 **Western blot of succinate dehydrogenase in C2C12 cells**

380 Following TCAP-1 treatments, proteins were extracted from C2C12 cells and lysed with
381 radioimmunoprecipitation assay (RIPA) buffer supplemented with the protease inhibitor,
382 phenylmethylsulfonic fluoride (PMSF) (Cell Signaling Technology, MA USA) and measured
383 using a bicinchonic acid (BCA) protein assay (Pierce BCA Protein Assay; Thermo-Fisher
384 Scientific, Toronto, Canada). All protein extracts were re-suspended in sample buffer and size-
385 fractioned by SDS-PAGE, electro-transferred to nitrocellulose membranes. Afterwards,
386 membranes were incubated with the succinate dehydrogenase (SDH) primary antibody and
387 subsequently treated with secondary antibody conjugated with chemiluminescent tags (Table 2).
388 Following TCAP-1 treatments, C2C12 cells were lysed with 500 µL of RIPA buffer supplemented
389 with PMSF. Cells were harvested and centrifuged at 20,000 rcf for 20m at 4°C. Protein
390 concentrations (as described above) were measured to standardize the dilutions of respective
391 supernatant samples. Samples (15 µg) were re-suspended in sample buffer and size-fractioned by
392 SDS-PAGE (10%) at 100V for 1h. The protein extract was electro-transferred to Hybond-ECL
393 nitrocellulose membranes (Amersham) for 2h at 100V. Membranes were washed 3x with PBS and
394 blocked in 5% milk-PBST (5% w/v non-fat milk powder in PBS with 0.2% Tween20; PBST) at
395 RT for 1h, then incubated with primary antibodies in 1% milk-PBST OT at 4°C. The membranes
396 were washed 3x in PBST at RT and incubated with a horseradish peroxidase (HRP)-conjugated
397 secondary antibody (VWR, Amersham; diluted to 1:7500 in 1% milk-PBST) for 1h at RT then

398 washed 3x in PBST at RT. The proteins were detected by adding chemiluminescence detection
399 reagent (ECL Amersham) to the membranes and exposing onto ECL Hyperfilm (VWR) for 30m.

400 **Diacylglycerol (DAG) and inositol triphosphate (IP3) assays**

401 The protocols provided by commercial DAG and IP3 assays (MyBiosource, San Diego,
402 California, USA) were followed. To determine the downstream Ca^{2+} response, 6 replicates of
403 C2C12 cells were prepared using the TCAP-1 treatment protocol described above then treated with
404 either vehicle, the IP3R antagonist, 2-APB, or the phospholipase C inhibitor, U73122. Cell lysates
405 were added to a microELISA plate coated with purified mouse DAG or IP3 antibodies.
406 Subsequently, 3,3',5,5'-tetramethylbenzidine (TMB) solution was added to detect the HRP-
407 conjugates as colour changes. Finally, sulphuric acid (0.01N) was added to terminate the reaction.
408 The absorbance change was measured at 450 nm by spectrophotometry (SpectraMax Plus, NH,
409 USA). For the IP3R inhibitor, 2-APB (100 μM) was applied before the start of treatment with
410 either sham (Locke's buffer with scTCAP-1) or TCAP-1 (100 nM). For live-cell fluorescence
411 experiments, C2C12 cells were differentiated and intracellular Ca^{2+} flux was assessed via fluo-4
412 via a flow-through bath chamber of an inverted microscope. Cells were quantified with a GFP
413 filter set at 480 nm with the fluorescence emission measured at 516 nm.

414

415 **Mitochondrial Ca^{2+} accumulation and membrane potential measurement in C2C12**
416 **myotubules**

417 Changes in mitochondrial Ca^{2+} levels were assessed using fluorescent indicator, Rhodamine-2-
418 AM (Rhod-2). C2C12 myotubules were loaded with Rhod-2 by incubating coverslips in DMEM
419 containing 4μM Rhod-2 (from a 1mM stock solution in DMSO with 20% pluronic; Invitrogen-
420 Pluronic™ F-127) for 30m at 22°C. Cells were washed once for 30m at 37°C in Locke's Buffer

Cells then acclimated for 15m at 22°C. To assess changes in mitochondrial Ca^{2+} levels, cells were continuously perfused in a flow-through chamber as indicated previously. Changes in Rhod-2 fluorescence was imaged using a TRITC filter set (Semrock, Rochester, NY, USA) and an X-Cite 120 fluorescence illumination system (Quorum Technologies, Inc. Guelph ON, Canada). Emissions were detected using an Orca-ER Hamamatsu BW CCD digital camera as described above. Rhod-2 was excited at 552nm every 100 ms and measured at 577nm. Multiple ROI were taken from the nuclear regions of the myotubules (n=5, 5-7 ROIs per coverslip). Changes in mitochondrial membrane potential were assessed using R123-based fluorescence. C2C12 myotubules were prepared with by incubating a coverslips in DMEM containing 5 µM R123 for 30m (37°C) followed by a 15m wash in Locke's Buffer. Changes in R123 fluorescence was imaged using the green GFP filter set using the same experimental configuration as previously described. R123 was excited with a wavelength of 480 nm for 100 ms every 5s and fluorescence emission was measured at 516 nm.

SiRNA knockdowns (KD) and CRISPR Knockouts (KO) of LPHN-1 and -3

For the siRNA KD studies, transfection with siRNA oligonucleotides was performed after 4d of C2C12 differentiation using Dharmacon SmartPOOL (Horizon Inc. Canada) siRNA for LPHN1 (L-061299-00-0005), LPHN3 (L-040779-00-0005) and a non-targeting control (D-001810-10-05). Dharmacon SmartPOOL siRNAs targeted against LPHN-1 and-3, glyceraldehyde-3-phosphate (GAPD) and a non-targeting control were re-suspended in 1x siRNA buffer from 20 µM stocks. The stocks were diluted in serum-free and antibiotic-free DMEM to 250 nM. A 7.5µL aliquot of Mirus TranslT-X2 (Mirus Bio LLC) transfection reagent was diluted in 200 µL serum- and antibiotic-free DMEM and incubated at RT for 30m. The mixture was added to C2C12 cells (see

444 above) with a final siRNA concentration of 25 nM. The cells were differentiated in siRNA-
445 containing media for 2d for a total of 6d of differentiation before use in the experiments. For
446 CRISPR studies, single-guided RNA (sgRNA) constructs were designed to target the mouse
447 LPHN-1 and -3 gene at 3 locations (see Fig. 2). C2C12 cells were transfected with sgRNA
448 constructs (Fig. 2C) and a Cas9 plasmid, generating heterogenous pools of transfected cells. The
449 CRISPR/Cas-transfected C2C12 cells (either hetergenous pools or clones) were trypsinized and
450 pelleted for DNA extraction. Genomic DNA was extracted using Lucigen QuickExtract DNA
451 extraction solution (Biosearch Technologies, Inc) according to the manufacturer's direction. The
452 LPHN-1 and -3 genes were amplified by PCR and digested by T7 endonuclease using the EnGen
453 Mutation Detection Kit (New England Biolabs) according to directions in combination with the
454 custom primers that flank the appropriate CRISPR-targeting regions (Fig. 2C). The fragments were
455 identified as previously described above. Clones that showed low or no WT PCR amplicon were
456 screened for LPHN1 expression by qRT-PCR. Selected clones showing significantly reduced
457 LPHN1 mRNA expression by qRT-PCR and western were termed 'LPHN1 E5U KO' and 'LPHN1
458 E5D KO' based on the exon position of mutated site and were used for further study (Fig. 2). The
459 activity of the clones were determined by TCAP-1-induced cytosolic Ca^{2+} flux in the manner
460 described above. Peroxisome proliferator-activated receptor γ coactivator 1α (PGC-1α) expression
461 in C2C12 cells was determined using the qRT-PCR methods described above.

462

463 **Figure 2. CRISPR-based targets for the mouse LPHN-1 and -3 genomic sequences. A.**
464 Schematics of LPHN-1 and -3 genomic organization. The oligonucleotides targeting these regions
465 are indicated as arrows. **B.** Sequence of the oligonucleotides used in the CRISPR knockdowns as
466 indicated in 'A' above.

Statistical Analyses

All data on graphs are represented as mean ± SEM. All data were analyzed by Student's t-test or one or two-way ANOVA, as described within each figure caption. Tukey's post-hoc test and Sidak's post-hoc test were used to determine significance in one-way and two-way ANOVA analyzes, respectively. An *a priori* hypothesis of $p<0.05$ was used as a threshold for statistical significance. GraphPad Prism 7-8 was used to analyze each statistical test.

Results

The primary structure of rat and mouse TCAP-1 possesses a high degree of homology among the other three paralogues (Fig 1A). Because the primary structure of rat and mouse TCAP-1 is identical, it was used for all studies, as well as a proxy for the other TCAP isoforms. The first studies completed established that the teneurins, TCAP and LPHNs could be expressed in rat skeletal muscle. Secondarily, the physiological role of TCAP-1 in rat skeletal muscle was examined.

In Vivo Rat Studies

In rat TA muscle mRNA extracts, all 4 teneurin mRNAs were identified based on the PCR primers indicated in Table 1. Teneurins-3 and-4 showed the strongest response, although both teneurins-1 and -2 were present, albiet weakly expressed. In contrast, TCAP-1 and -2 showed a strong signal relative to that indicated by teneurins-1 and -2 whereas TCAP-4 showed a signal consistent with teneurin-4. Although these studies were not quantitative, they do establish that both teneurins and

TCAP paralogues are present in rat skeletal muscle. However, importantly, both LPHN-1 and -3 cDNA bands were also strongly expressed, although there was no evidence of LPHN-2 in this preparation (Fig 3A).

Figure 3. Expression of the teneurin/TCAP-LPHN immunoreactivity (ir) in rat skeletal muscle: A. PCR expression of teneurins, TCAP and LPHNs in rat TA muscle. **B.** Immunological expression of β-dystroglycan, teneurin and LPHN in rat skeletal muscle. Arrows indicate nodes of aggregation (Scale bar: 100 μM). **C.** Enhanced examination of ir-LPHN regions in TA muscle cells. Left panel scale bar indicates 100 μM, whereas the right panel scale bar indicates 50 μM. Black arrows indicate cells with high LPHN-1 labelling, whereas white arrows indicate cells of low LPHN-1 labelling. **D.** Quantification of ir-LPHN-1 as a function of muscle cell diameter (size) as shown in 'C' (Student's t-Test $p<0.0001$; ****). **E.** Changes in fiber type in short-term TCAP-1 administration (t-test indicated for each pair). **F**. Changes in fiber-type over long term TCAP-1 administration (t-test indicated for each pair).

To corroborate these cDNA studies, immunohistochemical (IHC) studies were performed in rat TA muscle tissue. Initially, β-dystroglycan (DG) labelling was used to establish the sarcolemmic boundary of the cells, as previous studies indicated a relationship between DG and TCAP signaling [33]. Further, IHC co-localization labeling of Teneurin-1,-3 -and LPHN-1 was utilized to establish the cellular anatomical relationship between the teneurins and LPHNs. Immunoreactive (ir) teneurin-1 did not show a strong signal (data not shown), consistent with the RT-PCR data indicated above, however the ir-teneurin-3 showed a clear response indicating specific nodes of aggregation in the sarcolemma (Fig. 3B). Importantly, ir-LPHN-1 labelling of these tissues showed co-localization with the ir-DG along with ir-teneurin and ir-TCAP labelling consistent with the

PCR studies indicated in Fig. 3A. The variation among the PCR and ir-teneurin -1 and -3 expression was expected due to affinity differences among the antibodies and primers (see discussion). Moreover, these studies establish a clear relationship between TCAP, teneurins and LPHNs in rat skeletal muscle (Fig. 3B). Morphological differences, with respect to cross-section diameter between the vehicle- and TCAP-1-treated animals could be established. Thus, TCAP-1 administration induced a 25% increase ($p<0.001$) between the number of small and intermediate cells relative to the untreated vehicle rats (Fig. 3C, D). Because small and intermediate fibers are typically oxidative muscle fibres, these observations suggested that TCAP could stimulate glucose uptake in skeletal muscle. To corroborate these findings, the expression of myosin heavy chain (MHC) was evaluated in the TA muscle of both short-term and long term TCAP-treated animals. In both cases, there was a significant ($p<0.01$) 3- to 3.5-fold increase in the expression of the MHCI fibres in the TCAP-1-treated animals compared to the non-treated vehicle, although significant ($p<0.05$) differences were also observed among MHCIIa, MHCIIx and MHCIIb expression among the treated and untreated animals (Fig. 3E,F).

Taken together, these studies indicated that TCAP-1 may increase glucose transport into skeletal muscle. Therefore, TCAP-1-induced glucose uptake into the hind-limb was measured directly by fPET. Thus, using ^{18}F-deoxyglucose (FDG), a single dose of SC TCAP-1-treatment-induced FDG uptake in the hind-limb muscle by 2-fold ($p<0.05$) (Fig. 4.A,B) after 3d of treatment relative to vehicle treatment. These data corroborated our supposition that TCAP-1 acted, in part, to increase glucose importation into skeletal muscle. If this was the case, then this increase in glucose importation should increase skeletal muscle NADH production as a result of 2-glyceraldehyde-3-phosphate conversion to 2-1,3 diphosphoglycerate and secondarily through elements of the tri-carboxycyclic (TCA) acid cycle in the conversion to pyruvate. TCAP-1-treated muscle significant

536 ($p<0.05$) increased NADH-staining compared to vehicle (Fig. 4C, D) supporting increased TCAP-
537 1-mediated glucose transport.

538

539 **Figure 4. Glucose uptake and metabolism in rat hind-limb and TA muscle**. **A.** Function
540 positronic emission tomography (fPET) of rat hind limb showing increase of ^{18}F-deoxyglucose
541 (^{18}F-DG) uptake after 3 days from TCAP-1 administration. **B.** Quantification of the ^{18}F-DG uptake
542 in hindlimb after 3 days. (n=5; student's t-test; $p<0.05$). **C.** Stimulation of NADH in TA muscle
543 after administration of TCAP-1. Above panel, (hematoxylin and eosin stain), bottom panel, NADH
544 activity (shown as black regions). Scale bar indicates 100 µM. **D.** Quantification of the NADH-
545 labelled cells shown in 'C'. * $p<0.05$; **$p<0.01$; ***$p<0.001$; ****$p<0.0001$. Mean ± SEM
546 indicated n=4.

547

548 Muscle performance is related to the amount of energetic substrates available, therefore, we
549 examined the role of TCAP-1 on muscle activity *in vivo* in rats by determining the efficacy of
550 TCAP-1-mediated contractility using electrical stimulation of the TA muscle. After a 5-d daily
551 treatment of either vehicle or TCAP-1, following a 3-d washout period, muscle contractility was
552 assessed. TCAP-1-treated animals showed improved muscle dynamics. TCAP-1-treated animals
553 exhibited enhanced baseline contraction kinetics with respect to increased peak twitch force
554 ($p<0.05$) (Fig. 5 A,B), slower contraction velocity ($p<0.05$) (Fig 5C), and potentially higher faster
555 relaxation rates (Fig. 5D) compared to vehicle-treated animals. Following baseline measurements,
556 a 6-m fatigue protocol was induced in the muscle where contractile kinetics were recorded at 0, 1,
557 and 5m after the fatigue protocol. TCAP-1 enhanced recovery from the twitch stimulation (Fig.
558 5E-G). Although TCAP-1 did not influence peak twitch force (Fig. 5E), it significantly ($p<0.05$)
559 maintained twitch max dx/dt (Fig. 5F) and 1/2RT (Fig. 5G) over the course of the fatigue protocol

which was diminished in vehicle-treated animals. All data was normalized to muscle mass. The treatment did not affect muscle mass (Fig. 5H), tetanic force (Fig. 5I) or the fatigue force curve (Fig. 5J). Thus, TCAP-1 enhanced the efficiency of the existing muscle morphology, rather than increasing muscle mass, and maintained contraction cycling efficiency during fatigue. To assess the effects of a long-term (LT) treatment, rats were administered either vehicle or TCAP-1, for 3 months (1 injection/week). Two weeks post-treatment, the TCAP-1-treated animals elicited a comparable peak twitch force to vehicle-treated animals (Fig. 5K-J), however had significantly ($p<0.05$) slower contraction velocity and faster ($p<0.05$) relaxation rate (Fig. 5L,M).

Figure 5. *In vivo* actions of TCAP-1 on rat TA muscle kinetics. A-J. Muscle twitch kinetics after animals treated with TCAP-1 once a day for 5 days before testing **A**. Representative twitch traces (black, vehicle; gray, TCAP-1). **B**. Baseline contraction kinetics (t-test). **C.** Contraction velocity (t-test). **D.** Relaxation rate (t-test). **E.** Peak twitch force (2-way ANOVA). **F.** Twitch max dx/dt (2-way ANOVA). **G.** 1/2RT analysis (2-way ANOVA). TCAP-1 treatment did not affect muscle weight (t-test) (**H**), tetanic force (t-test) (**I**) or fatigue force over time (**J**) (n=7-8). **K-M.** Long term treatment of TCAP-1 on rat hind-limb twitch kinetics. **K.** contraction max dx/dt. **L.** 1/2RT rate. **M.** Relaxation rate.

In Vitro Mouse Cell Studies

The initial PCR screen of C2C12 cells indicated that, although only teneurin-3 was highly expressed (Fig.6A), all 4 TCAP transcripts could be discerned (Fig. 6B). In both undifferentiated C2C12 myoblasts, and 6-d myotubules, the transcripts for LPHN-1 and -3 were present (Fig. 6C). IHC expression of TCAP-1 showed a similar punctate expression in the cytosol of the C2C12

583 myoblasts (Fig. 6D) as we have previously shown for neurons [38] where FITC-labelled TCAP-1
584 was present at several sarcolemmic regions consistent with the expected expression of the receptor
585 [32,33,38]. Moreover, because TCAP-1 regulates actin organization and polymerization in
586 neurons [38], the C2C12 cells were treated with TCAP-1 and examined using the phalloidin stain
587 to highlight actin fibers (Fig. 6E). This resulted in a major increase in actin polymerization in the
588 TCAP-1-treated cells at both 30m ($p<0.01$) and 2d ($p<0.001$).

589

590 **Figure 6. Expression of teneurin, TCAP and LPHN in C2C12 myoblasts. A**. PCR-based
591 teneurin expression; **B**. PCR-based TCAP expression; **C.** PCR-based LPHN expression. **D.** C2C12
592 cells labelled with TCAP-1 antisera showing the difference between the endogenous ir-TCAP and
593 the presence of FITC-TCAP-1 localization. ir-TCAP-1 is indicated in red, whereas the DNA-
594 associated DAPI labelling is indicated in blue. FITC-labeled TCAP-1 is shown in green. Arrows
595 indicate regions of FITC-TCAP-1 uptake. Scale bars indicate 50 μM **E.** Actions of TCAP-1 on the
596 proliferation of the C2C12 myoblasts when treated with TCAP-1 at 30 minutes and 2 days. Actin
597 is indicated in red, whereas the nuclei are indicated in the DAPI-based blue. Scale bars indicate
598 100 μM.

599

600 Having established that TCAP-1 behaved in a similar manner as previously shown in neurons, the
601 viability of the Ca^{2+} response in the differentiated myotubules was evaluated to determine their
602 efficacy before proceeding to further studies. Initially, caffeine was used to determine the limits
603 of the Ca^{2+} response in the differentiated myotubules relative to the TCAP-1 response (Fig. 7A-
604 D). These studies indicated that the myotubules were active and viable, and with respect to the
605 Ca^{2+} response, did not show an appreciable decrease in cytosolic Ca^{2+} concentrations (Fig. 7B),
606 although it did attenuate the rate of cytosolic Ca^{2+} concentrations ($p<0.01$). Taken together, these

607 studies indicated that the myotubules were viable with respect to our preparation, and that the
608 attenuating TCAP-1 response indicated that additional regulating factors were likely present. Thus,
609 given these observations, the direct action of TCAP-1 on Ca^{2+} flux in myotubules was examined
610 (Fig. 7E-H). TCAP-1 increased Ca^{2+} concentrations by almost 4-fold relative to the control-treated
611 cells ($p<0.001$).

612

613 **Figure 7. Caffeine- and TCAP-1- mediated Ca^{2+} response in differentiated C2C12 myocytes.**
614 **A**. Heat-map images showing the Ca^{2+} response induced by caffeine, TCAP-1 or vehicle. Mean
615 and SEM is indicated**. B**. Dynamic concentration changes over the period of analysis shown in
616 'A'. Mean ± SEM is indicated**. C.** Total concentration changes of the manipulations of the study
617 period indicated in 'A'. **D.** Rate of Ca^{2+} release between caffeine and TCAP-1. **E.** TCAP-1
618 mediated Ca^{2+} actions show normal morphology in cells. **F.** Rate of increase in Ca^{2+}-associated
619 fluorescence after administration of TCAP-1. **G.** Quantification of the change in TCAP-1 mediated
620 intracellular Ca^{2+} concentrations indicated in 'F'. Significance was determined by a Students t-
621 test. (* $p<0.05$; **$p<0.01$; ***$p<0.001$; ****$p<0.0001$. Mean ± SEM indicated n=4).

622

623 In skeletal muscle, the predominant glucose transporter protein (GLUT) isoform is the insulin-
624 sensitive GLUT4 protein. Using insulin as a control, a significant ($p<0.001$) increase in the
625 expression of the ir-GLUT4 transporters was observed for both TCAP-1 and insulin treatments
626 over 30m (Fig. 8 A,B) in C2C12 cells. To determine whether this GLUT4 response was dependent
627 on the TCAP-1-mediated Ca^{2+} release, the IP3R antagonist, 2-APB, that abolishes the TCAP-1
628 Ca^{2+} response, was investigated. In the presence of the inhibitor, both TCAP-1 ($p<0.01$) and insulin
629 ($p<0.001$) inhibited the ir-GLUT4 expression (Fig. 8A,C). This importation of glucose by TCAP-1
630 was further corroborated in C2C12 cells showing that TCAP-1 significantly ($p<0.0001$) induced

631 ^{3}H-2-deoxyglucose increase into the cytosol over 30m, similar to that of insulin (Fig. 8D).
632 However, both peptides show distinct glucose-uptake profiles, where insulin induces a significant
633 increase at 30m ($p<0.001$), 45m ($p<0.001$) and 60m ($p<0.01$), whereas TCAP-1 induces an
634 increase at 30m ($p<0.001$) but was attenuated by 45m ($p<0.01$) and returns to baseline at 60m. The
635 sc-TCAP-1 treatment, used separately as a negative peptide control in this study, showed no
636 significant change from the saline vehicle.

637

638 **Figure 8: TCAP-mediated glucose metabolism in C2C12 cells. A**. Regulation of ir-GLUT4 by
639 TCAP-1 and insulin myotubules. Red indicates ir-GLUT4 whereas blue shows DAPI staining of
640 the nuclei. Arrows indicated regions of high immunoreactivity. Scale bar=100 µM. **B**.
641 Quantification of ir-GLUT4 expression over 30 minutes. **C**. Effect of the IP3R inhibitor, 2-APB
642 on TCAP-1- and insulin-mediated ir-GLUT4 labelling. **D.** Uptake of ^{3}H-2-deoxyglucose in C2C12
643 myoblasts by TCAP-1 and insulin. **E.** Changes in static ATP concentrations following treatment
644 by TCAP-1. **F.** NADH production increase as determined by a resesourin assay following TCAP-1
645 treatment relative to the vehicle. **G**. Increased ir-succinate dehydrogenase expression after 1 hour
646 following TCAP-1 treatment as determined by western blot. **H.** Quantification of the data indicated
647 in 'G'. Significance was determined by a t-test as indicated in C, F and H or one-way ANOVA
648 shown in B D and E. (* $p<0.05$; ** $p<0.01$; *** $p<0.001$; **** $p<0.0001$. Mean ± SEM indicated
649 n=6).

650

651 Increased glucose importation increases ATP and NADH turnover in cells due to glycolytic and
652 tricylic acid (TCA) cycle activity. Therefore, this was examined with respect to TCAP-1 treatment.
653 As a result, both ATP ($p<0.001$) (Fig. 8E) and NADH ($p<0.001$) (Fig. 8F) turnover were
654 significantly increased after 30m of TCAP-1 treatment, although NADH levels remained about
655 60% higher ($p<0.001$) than vehicle levels after 60m. Moreover, succinate dehydrogenase (SDH; a

rate-limiting step of the TCA cycle) protein expression was increased by over 2-fold after TCAP-1 treatment corroborating the previous experiments of increased ATP and NADH production ($p<0.05$; Fig. 8G,H).

As we have previously established that the IP3-DAG pathway is important for TCAP-1-mediated intracellular Ca^{2+} flux in neurons, this pathway was examined in C2C12 cells. Relative to the vehicle, TCAP-1 induced a significant increase at 5 and 15 min ($p<0.001$; Fig. 9A) in intracellular DAG concentrations and a major increase between 1 and 15 min ($p<0.0001$; Fig. 9B) in IP3 concentrations. To confirm this action, TCAP-1-treated C2C12 cells were blocked with either the IP3R antagonist, 2-APB, or the phospholase C inhibitor, U73122. The 2-APB and U73122 treatment reduced TCAP-1-mediated Fluo-4 concentrations to about 30% ($p<0.01$) of their original values indicating that the IP3-DAG pathway plays an active role in increase of TCAP-1-mediated intracellular Ca^{2+} flux (Fig. 8C,D). Because this TCAP-1-mediated rise in intracellular Ca^{2+} concentrations can target the mitochondria [39], the mitochondrial Ca^{2+} dye, rhodamine 1-AM (Rhod-2) was utilized to determine the concentration of Ca^{2+} sequestration in mitochondria. There was a 5-fold increase ($p<0.001$) in Rhod-2-associated Ca^{2+} labelling over 200s (Fig. 9E,F). Related to this, Rhod-123, was used to determine the level of mitochondrial polarization. TCAP-1 treatment significantly decreased Rhod-123 fluorescence ($p<0.001$) relative to vehicle indicating depolarization of the mitochondria membrane (Fig. 9G, H).

Figure 9. TCAP-1 mediated calcium regulation in C2C12 cells. A. TCAP-1 mediated increase in intracellular DAG concentrations (mean and SEM shown; n=6). **B.** TCAP-1 mediated increase in intracellular IP3 concentrations (mean and SEM shown; n=6). **C.** Increase in intracellular TCAP-1 mediated Ca^{2+} concentrations and inhibition by the IP3 receptor (2-APB) and

679 phospholipase C (U73122) antagonists; **D.** Quantification of data shown in C (n=6). **E.** Uptake in
680 Ca^{2+}-mediated Rhod-2 into mitochondrial membranes. **F.** Quantification of data shown in E based
681 on the change at 200 seconds. **G.** Decrease in Rhod-123 immunofluorescence in mitochondrial
682 membranes as a result of TCAP-1 administration. This decrease in Rhod-123 indicates a decrease
683 in mitochondrial membrane depolarization. **H**. Quantification of the data indicated in G based on
684 the changes at 225 seconds. (* $p<0.05$; **$p<0.01$; ***$p<0.001$; ****$p<0.0001$.)

685

686 Although these studies are similar with previous investigations of teneurins, TCAPs and LPNHs
687 in neurons, this is the first study to examine teneurin/TCAP and LPHN activity in skeletal muscle
688 function. To determine whether the TCAP-1 activation was dependent upon the LPHN receptors,
689 these genes were knocked-down (KD) using siRNA oligonucleotides, or knocked-out (KO) using
690 CRISPR in the C2C12 cells. Using the C2C12 cells, the LPHN-1 and -3 expression was reduced
691 using the siRNA oligonucleotides. The LPHN-1 receptor mRNA was reduced about an 80%
692 ($p<0.01$) relative to the WT cells. Transfection with either the LPHN-1 siRNAs or the null vector
693 (NT) did not significantly change mRNA expression relative to the WT control (Fig. 10A).
694 Similarly, the LPHN-3 siRNA-associated oligonucleotides significantly ($p<0.01$) decreased its
695 mRNA expression about 65% relative to the WT cells. There were no significant changes in
696 mRNA expression of the LPHN-1 transcript in either the LPHN-1 KD or the NT cells (Fig. 10B).
697 Despite the reduced expression of these receptors, cell morphology was normal (Fig. 10C). TCAP-
698 1 increased cytosolic Ca^{2+} in cells transfected with the NT control, however, relative to the NT
699 control, TCAP-1 did not increase Ca^{2+} in either the LPHN-1 and -3 siRNA-transfected cells, which
700 showed a significant decrease ($p<0.01$ and $p<0.001$, respectively) in intracellular Ca^{2+}
701 concentrations (Fig. 10D,E). However, because both LPHN-1 and -3 siRNA oligonucleotides
702 unexpectedly reduced intracellular Ca^{2+} concentrations by similar amounts, we repeated this study

by ablating the LPHN-1 and -3 receptors using CRISPR methods. The E5U7 target reduced LPHN-1 expression by about 90% ($p<0.01$) whereas, the E5D3 target reduced mRNA levels by about 95% ($p<0.05$) relative to the WT cells (Fig. 11A). A significant decrease ($p<0.05$) in LPHN-1 mRNA levels were present in both sets of transgenic cells (Fig. 11B). Importantly, cell morphology was normal in the transgenic cells (Fig.11C). CRISPR-based KOs of the LPHN-3 gene were unsuccessful after numerous attempts (data not shown; see discussion), hence studies were performed with the LPHN-1 KOs only. Similar to that achieved using the siRNA knock-down cells, both CRISPR-associated KO transgenic cells (E5U and E5D) reduced intracellular Ca^{2+} levels by about 60% ($p<0.001$) (Fig.11 D,E). Taken together, both the siRNA- and CRISPR-associated methods to reduce mRNA expression indicate that the TCAP-1 associated intracellular Ca^{2+} flux was mediated primarily by its interactions on LPHN-1 and -3.

Figure 10: siRNA knockdown of LPHN-1 and -3 in C2C12 cells. A. Cells transfected with the LPHN-1-targetting siRNAs showed a significant reduction ($p<0.01$) in LPHN-1 mRNA expression. **B.** Cells transfected with the LPHN-3 targetting mRNA significantly ($p<0.01$) reduced LPHN-3 mRNA expression. **C.** Cells treated with either siRNAs showed normal morphology. **D.** Changes in Ca^{2+} accumulation in cells transfected with either LPHN-1 or -3 siRNA oligonucleotides. **E.** Quantification of the data shown in 'D' at 200 seconds.

Figure 11: .CRISPR-based knockouts of the LPHN-1 and -3 genes in C2C12 cells. The two clones (E5U7) (**A**) and (E5D3) (**B**) significantly reduced LPHN-1 expression relative to NT and WT cells. **C**. The morphology of the C2C12 cells were normal in both transfected cell lines. **D**. Changes in cytosolic Ca^{2+} accumulation in the various cell types. **E.** Quantification of the data shown in 'D' after 200 seconds. **F, G, H,I.** Changes in NADH production as determined by the resasurin assay **. J.** Quantification of the data shown in F-I, K. Reduction in PGA-1α mRNA

727 expression by PCR in E5U7 and E5D3 clones. * $p<0.05$; **$p<0.01$; ***$p<0.001$; ****$p<0.0001$.
728 Mean ± SEM indicated n=7-8.

729

730 To corroborate these findings with the previous observations that TCAP-1 could regulate energy
731 metabolism in skeletal muscle cells, the action of TCAP-1 on NADH production via a resazurin
732 assay was performed on the CRISPR LPHN KO cells (Fig 11F-I). From 30-150m, the TCAP-1-
733 treated WT C2C12 cells showed a significant increase ($p<0.01$; $p<0.05$, respectively) in
734 fluorescence compared to the vehicle (Fig. 11F). LPHN-1 E5U7 (Fig. 11G) and E5D3 (Fig.11H).
735 KOs did not show an increase after TCAP-1 treatment, whereas the NT control cells showed a
736 significant ($p<0.01$ increase after 120m (Fig. 11I). FCCP treatment, indicating cell viability
737 induced significant increases ($p<0.001$; $p<0.0001$) across all cell types (Fig. 11 F,G,H,I).

738 Given that the *in vivo* studies showed that TCAP-1 can modulate MHCI and that TCAP-1 may
739 also affect other hormones and signalling factors, it was unclear if the purported fibre changes
740 observed in TA muscle was a direct result of TCAP-1. Therefore, because PGC-1α is a
741 transcription factor that up-regulates MHCI expression [46], the TCAP-1 actions on PGC-1α was
742 measured by qRT-PCR. Following the TCAP-1 treatment (100nM), neither the E5U7 nor the
743 E5D3 cells showed any significant increases, whereas, both the WT cells and NT controls showed
744 about a 50% increase ($p<0.05$) in PGC-1α expression (Fig. 11K). This indicated that TCAP-1 has
745 the potential to directly influence MCH fibre expression at the transcriptional level.

746

747

748

Discussion

This study describes a novel mechanism underlying skeletal muscle physiology. This investigation is the first to show a functional relationship between teneurins and latrophilins (LPHN) with respect to skeletal muscle function in mammals using rodent models. We have previously established that there is a functional peptide on the distal tip of the teneurin extracellular region which we have termed 'teneurin C-terminal associated peptide' (TCAP) and is highly active in the CNS. Now, our data indicates that TCAP-1 affects skeletal muscle strength and fatigue, *in vivo,* via a glucose-associated and, likely, an aerobic mitochondrial-based mechanism. This mechanism is consistent with our previous findings in neurons and the CNS. Moreover, TCAP-1 interacts with the putative teneurin receptors, LPHN-1 and -3 to activate the PLC-IP3-DAG pathway to regulate intracellular Ca^{2+} flux that ultimately regulates glucose importation and mitochondrial activity. The hypotheses developed from the *in vivo* studies were subsequently tested *in vitro* utilizing the rat skeletal cell line, C2C12, to establish a cellular model upon which to base the *in vivo* actions of TCAP-1 with respect to skeletal muscle dynamics.

A critical aspect of this study was the utilization of TCAP-1 as a peptide analogue of the distal C-terminal region of teneurins. The genomic structure of the TCAP region of teneurins indicated that it possessed a potentially cleavable peptide [22,24]. A synthetic version of TCAP-1 was developed by replacing the N-terminal glutamine with pyroglutamyl acid and amidating the C-terminal residue [24]. The resultant synthetic peptide was highly efficacious at regulating neural function, behaviour and reproductive physiology in rodents [24,31,33,36-38] indicating that TCAP-1, itself, possessed independent biological functions. Thus, rat/mouse TCAP-1 was utilized in this study based on our previous work with this peptide. As indicated in Fig.1, the primary structure of rat and mouse TCAP-1 is identical, and consequently, the same peptide was utilized for all *in vivo*

772 and *in vitro* experiments. However, it is important to point out that, although there are four
773 paralogous forms of teneurins and TCAP in vertebrates, albiet, with significant primary structure
774 conservation among them, our study has utilized only TCAP-1. TCAP-1 was utilized, therefore,
775 as a proxy for all TCAPs present in the organism or tissue, to determine the potential to regulate
776 skeletal muscle function. Based on our previous studies of this peptide and its level of primary
777 structure conservation, evidence indicates that our supposition is valid.

778 Elucidation of the teneurin/TCAP-LPHN network is complex. To date, there are 4 teneurins found
779 in vertebrates, each of which possesses a TCAP at its extracellular tip [4,17,18,23,24,26].
780 Moreover, the 3 latrophilin paralogues (LPHN1-3) have been identified in the vertebrate genome
781 [29,47,48]. A clear stoichiometry among teneurins and the LPHNs has been only partially
782 resolved. Both ligand and receptor proteins possess multiple domains that interact with a variety
783 of peripheral ligands in the extracellular matrix, the membrane and intracellularly as well
784 [10,13,14,21,22]. TCAP, as an amphiphilic peptide, that may be cleaved [14,22], or expressed
785 separately [33,34] is a 'wild-card' in this perplexity of molecular interactions. Although TCAP is
786 clearly bioactive with respect to cytoskeletal reorganization [32,33,37,38], glucose regulation
787 [3,39], signal transduction [24,38,39,49], metabolism [24,32,34,39] and stress-associated
788 behaviour [36, 50-54], these studies have focused at the neurological level. Despite this emphasis,
789 few studies [55] regarding the role of teneurins/TCAP and LPHN on skeletal muscle physiology
790 have been reported.

791 Our goal in examining the role of TCAP-1 and LPHN-1 and -3 was not intended to establish a
792 specific molecular interaction, per se, but rather to show that the teneurin/TCAP-LPHN system
793 plays an important role in skeletal muscle metabolism. Consequently, our investigation that
794 paralogues of teneurins, TCAPs and LPHNs were present both in hind-limb skeletal muscle

preparations and in C2C12 cells provided the basis of this molecular system with respect to skeletal muscle physiology. Because TCAP-1 co-localization to cell membranes was associated with the dystroglycan (DG) complex [38], we used DG antibodies to delineate the sarcolemma. In this study, the interaction of the teneurin-3 and LPHN-1 in the TA muscle occurred at specific nodes in the sarcolemma rather than being spread throughout all regions of DG labelling (see Fig. 3B). Our data indicates that teneurin-3 is the dominant teneurin in skeletal muscle tissue. However, the antisera available for the teneurins limited us to visualize histochemically only teneurin-3-like epitopes, although PCR expression indicated that the teneurin-3 transcript was expressed. All 4 TCAPs were expressed by PCR although TCAP-3 showed low expression. In contrast, expression of these transcripts in C2C12 cells indicated high expression of teneurin-3 along with all 4 TCAPs (see Fig. 6A,B). This is the first time we have observed high TCAP expression without the corresponding teneurin expression using PCR (Lovejoy, unpublished observations), although we have only focused on neurons previously. We acknowledge that it can be difficult to reconcile the expression patterns of teneurins using the antibodies available at the time, however, it is important that both elements are present. These data may indicate a fundamental difference among teneurin and TCAP expression in skeletal cells relative to neurons.

Our data indicated that TCAP-1, like in neurons [39], regulates glucose-mediated aerobic-based energy metabolism in skeletal muscle. Several observations support this hypothesis. First, *in vivo*, ir-LHPN primarily labeled small and intermediate muscle fibres in the rat TCA muscle (see Fig. 3C,D), that are typically associated with aerobic action. Second, with respect to MHC proteins, TCAP-1 showed the greatest increase in MCHI expression in both short-term and long-term TCAP-1 treatment of rats. Muscle kinetics are dependent, in part, on the relative proportion of muscle fibers types. Although the TA muscle consists of 95% type-II muscle (fast-twitch

818 glycolytic muscle fiber type), TCAP-1 imparts traits of type-I fibers (slow-twitch and oxidative)
819 which possess greater MHC expression. Importantly, both short-term ($p<0.01$) and long-term
820 TCAP-1 ($p<0.01$) administration (Fig.3 E,F) increased in the MCHI fibre expression, although in
821 short-term TCAP-1- treated animals, MHCII expression was specifically decreased in MHCIIa,
822 ($p<0.05$); MHCIIx ($p<0.01$) and MHCIIb ($p<0.05$) mRNA expression, where only MHCIIB
823 showed a decrease ($p<0.01$) in the long-term treated rats. These expressional changes of MHC
824 transcription were corroborated by the expression of PGC-1α, a critical transcriptional co-factor
825 that regulates the mitochondrial actions of myosin chain transcription. Using the C2C12 cells as a
826 model, TCAP-1 increased the transcription of PGC-1α and was inhibited ($p<0.05$) by CRISPR-
827 mediated KOs of the LPHN-1 gene. Thus the TCAP-1-mediated Ca^{2+} surge may activate CaMKIV
828 and CaN transcriptional regulators to promote the transcription of PGC-1α. Overall, this indicates
829 that TCAP-1 is increasing slow-twitch gene expression, consistent with the *in vivo* contractile
830 kinetics observed in Fig 5. Third, rats treated with TCAP-1 enhanced baseline contractile kinetics
831 under basal and fatigue conditions using both short- and long-term TCAP-1 administration. Fourth,
832 a single dose of TCAP-1 increased uptake of ^{18}F-2-deoxyglucose in rat hind-limb regions as
833 determined by fPET analysis. Fifth, because Ca^{2+} and ATP are required for proper muscle
834 contraction initiation and relaxation, TCAP-1 significantly increased GLUT4 expression (Fig.8A),
835 increased ^{3}H-2-deoxyglucose uptake (Fig. 8D), ATP (Fig. 8E) and NADH (Fig. 8F) concentrations
836 and increased the protein expression of SDH in the TCA cycle (Fig. 8G,H) using the C2C12
837 myoblasts and myotubules. Taken together, these studies support the hypothesis that TCAP-1
838 regulates glucose uptake and metabolism in skeletal muscle cells in a similar manner previously
839 described in neurons [39].

Glucose is the main energy nutrient for skeletal muscle function, thus, up-regulation of glucose metabolism could impact skeletal muscle activity. Therefore, the influence of TCAP-1 on these contractile kinetic parameters indicates that TCAP-1 modulates Ca^{2+} levels to enhance SR-sarcomere coupling. During fatigue, cytosolic Ca^{2+} levels accumulate due to inefficient SR-sarcomere coupling, thereby reducing muscle function as was observed in contractile kinetic parameters such as peak twitch force and 1/2RT. TCAP-1 treatment significantly increased both parameters, indicating a clear role in Ca^{2+} modulation. Moreover, these results also suggest that TCAP-1 increases ATP production rate to meet the energetic demands of the muscle during fatigue. After the contraction, Ca^{2+} is cleared from the cytosol and re-uptaken into the SR via the associated Ca^{2+} -ATPase (SERCA) pumps. SERCA pumps are high energy-consuming channels that account for 20-50% of the energy turnover in a single contraction cycle [43,56]. Prolonged stimulation results in the rapid depletion of ATP, thus reducing SERCA activity, ultimately leading to the accumulation of cytosolic Ca^{2+}. However, because TCAP-1 increases glucose uptake into the muscle, it provides additional substrates for energy metabolism which could maintain SERCA activity during fatigue. This is corroborated by the finding that TCAP-1 had significantly faster 1/2RT during fatigue compared to vehicle treatment and by the increase in the type-1 muscle fiber associated gene transcription that occurred in both short-term and long-term actions of TCAP-1.

From these studies, it is clear that TCAP-1 targets the mitochondria as it has potent actions upon Ca^{2+} modulation and glucose signaling. As TCAP-1 increases Ca^{2+} uptake into the mitochondria, likely from shuttling Ca^{2+} from the SR, this stimulates enzymes in the TCA cycle, specifically glycerol phosphate dehydrogenase, pyruvate dehydrogenase phosphatase, isocitrate dehydrogenase and oxoglutarate dehydrogenase [57,58]. This activates mitochondrial respiration via the ETC and leads to increased energetic output, as seen by increases in ATP, NADH and

SDH. Thus, this may explain enhanced metabolism and function results under TCAP-1 treatment. Previous studies in neurons have established that the IP3-DAG pathway is activated in response to TCAP-1. In this study, we showed that a similar situation occurs in C2C12 cells and, likely, in skeletal muscle. TCAP-1 treatment of C2C12 cells increase intracellular Ca^{2+} flux that can be blocked using IP3 receptor (2-APB) and phospholipase C (U73122) inhibitors. Moreover, this increase in intracellular Ca^{2+} is likely responsible for the depolarization of the mitochondrial membranes. This work supports a previous report that SR-associated Ca^{2+} release was directed toward the mitochondria in skeletal muscle [59].

These studies are consistent with previous observations in immortalized mouse neurons [39] and in zebrafish [34]. Although these previous studies indicate a relationship with TCAP-1 and LPHN action on Ca^{2+} flux involving the IP3-DAG pathway [39,60] other studies indicate that the LPHN-mediated AMP-PKA pathway may also be activated by teneurins and TCAP [61,62]. For example, TCAP-1 and -3 can increase cAMP levels in immortalized mouse neurons [24,37,49]. Further, studies of vertebrate teneurins have also implicated activation of the PKA- cAMP cascade [31]. However, our goal in this study was to establish a mechanism by which TCAP-1 can regulate energy metabolism in C2C12 cells, and for this reason we have focused on a Ca^{2+}-associated mechanism, as it aligns with previous studies. However, we acknowledge that given the complexity of teneurin-LPHN actions, other signal transduction systems such as ERK-MEK [38] are also likely required for the full set of teneurin- and TCAP-mediated LPHN actions on cells. Ancient-evolving peptide-protein systems will likely impinge on more than one intracellular signal cascade events because they evolved before many of the later intracellular signaling transducing pathways [31].

885 The mitochondria are ultimately responsible for supplying aerobic-based energy requirements to
886 eukaryotic cells. We have previously shown the relationship of TCAP-1 mediated energy
887 production and the mitochondria in the mouse neurons [39] and in zebrafish metabolism [34],
888 however this was the first study to establish the link between the teneurin/TCAP-LPHN system
889 and mitochondria in skeletal muscle cells. Although we have not studied mitochondria respiration
890 directly in this study, previously we showed that TCAP-3-treated zebrafish [34] increased both
891 basal and respiratory reserve capacity. Although total mitochondrial respiration is linked to proton
892 leak and ATP-linked respiration [63], no TCAP-3-associated actions on the latter could be
893 detected, but proton leak was increased in these studies.

894 The role of the teneurins, TCAP and LPHNs, together, has previously not been examined in
895 skeletal muscle. Therefore, we utilized both siRNA- and CRISPR-based methods to determine if
896 the reduced activity of the LPHN-1 and -3 receptors would attenuate TCAP-1-mediated
897 intracellular actions. Both CRISPR-based KOs of LPHN-1 significantly reduced the TCAP-1
898 associated increase in intracellular Ca^{2+}. We were unsuccessful to create a LPHN-3 KO however.
899 The length of the LPHN-3 gene in mice is about 10 times that of the LPHN-1 gene due to much
900 longer intronic sequences. Thus, this extended sequence may have played a role in the lack of
901 viability of the CRISPR- associated LPHN-3 oligonucleotides. Moreover, TCAP-1-mediated
902 intracellular Ca^{2+} was established using pharmacological antagonists of the PLC-IP3-IP3R
903 pathway of the SR. This rise in intracellular Ca^{2+} led to increased cellular glucose, concomitant
904 with increases in ATP and NADH production. Indeed, the TCAP-1-mediated increase in
905 intracellular Ca^{2+} corroborated with mitochondrial membrane hyperpolarization and increased
906 succinate dehydrogenase activity indicating that TCAP-1 also acted to increase mitochondrial
907 activity. However, the siRNA oligonucleotides did inhibit the actions of both receptors as

908 indicated by the significant reduction in the TCAP-1-mediated cytosolic Ca^{2+} response. siRNA
909 KDs of the LPHN-1 and -3 has been successfully used in the past using the mouse pancreatic β-
910 cell line, MIN6 [64] where the authors showed that LPHN-3 KDs reduced insulin secretion by
911 reducing cAMP levels via a Gi-mediated pathway. Although we have not examined the direct role
912 of TCAP-1 on pancreatic insulin release, this study is consistent with our supposition that TCAP,
913 itself, is associated with glucose regulation *in vivo* [3,39]. In our current study, however, our
914 experiments showed that ablation of LPHN-1 or -3 reduced TCAP-1-mediated Ca^{2+} concentrations
915 toward baseline levels. These results surprised us. We expected that the KO or KD or either
916 receptor would render only a partial suppression of the Ca^{2+} response. Because this was not the
917 case, one possibility is that there is an interaction among the LPHN isoforms specifically, or their
918 combined actions with the teneurins.

919 Teneurin and LPHN interaction is complex where the stoichiometry among the 4 teneurin and 3
920 LPHN paralogues has not been ascertained. Although studies using vertebrate models establish
921 clear evidence of teneurin-LPHN interaction [14,22,28,31], the specific correspondence of any
922 teneurin with any LPHN as cognitive pairs has yet to be established. The teneurins are
923 multifunctional transmembrane proteins that have TCAP at their distal extracellular tip. Even less
924 is understood regarding the promiscuity of the LPHNs with respect to TCAP interactions.
925 Previously, Silva and his associates [31] showed that the teneurin-2 region possessing the TCAP
926 unit was required for full binding to the LPHN-1 (Lasso), and Husic and her colleagues [32]
927 showed that the transgenic expression of teneurin-1 TCAP co-precipitated with the transgenic
928 over-expressed hormone binding domain (HBD) of LHPN-1 and, moreover, modulated the cell
929 adhesion characteristics of HEK293 cells overexpressed with the LPHN-1 mRNA. In this current
930 study, we established that both LPHN-1 and teneurin-3 transcripts were present and are co-

931 localized in the sarcolemma (Fig.3). These data corroborate with the PCR expression data
932 indicating that these mRNA transcripts show the highest expression, but are not meant to suggest
933 that this is indicative of cognitive ligand and receptor pairs, per se.

934 There is evidence that LPHN paralogues interact with each other. In our LPHN-1 and -3
935 attenuation studies, the reduction of one receptor inhibited the TCAP-1 mediated Ca^{2+} actions of
936 the other receptor. It is possible that there is a minor Ca^{2+} response mediated by the non-target
937 LPHN, but too low to detect with our assay conditions, although this seems unlikely. Homo-and
938 heterophilic oligomerization is a characteristic of the GPCRs, but this has not been well-studied in
939 Adhesion GPCR family members [65,66]. In LPHN-1, the C-terminal fragment and N-terminal
940 fragment is cleaved *in vivo* and re-associates with the α-latrotoxin (αLTX) mutant ligand LTX^{N4C}
941 [67], although this phenomenon has not been studied in detail in other LPHN paralogues despite
942 the high degree of conservation among these domains. Further, studies using the '*stachel*' peptide
943 have provided additional insight into potential LPHN paralogue interactions with each other
944 [64,68,69]. The *stachel* peptide represents the N-terminus of the C-terminal fragment following
945 cleavage of the conserved GPCR-autoproteolysis (GAIN) region [70]. The recombinant expressed
946 *stachel* peptide induces diverse G-protein associations across LPHN paralogues, whereas αLTX
947 favours G11 signalling via LPHN-1 [60,71,72]. We and others have previously shown that the
948 TCAP amino acid sequence resembles that of Secretin GPCR family ligands and αLTX [26], thus
949 we posit that TCAP may represent the endogenous ligand that αLTX co-evolved with to become
950 a toxin.

951 One of the questions we did not address in this study was the trigger that stimulates TCAP to
952 regulate skeletal muscle physiology. Our hypothesis, at this time, is that TCAP is liberated locally
953 in the sarcolemma either by a direct cleavage of the teneurin [14,22,23] or by independent mRNA

954 transcription, translation and release from skeletal muscle or other local tissues [33,34]. We have
955 shown in the past that TCAP-1 can increase teneurin transcription in immortalized neurons [24],
956 but we have yet to establish this *in vivo*. Although TCAP is highly expressed in the brain, our
957 studies showing its presence in as a circulating hormone in serum has been equivocal (Lovejoy,
958 unpublished observations). As this is a critical aspect of TCAP action, this is a goal for upcoming
959 studies.

960 In summary, our data in this study indicate that TCAP-1 regulates energy metabolism in skeletal
961 muscle via an insulin-independent mechanism, and by doing so, modulates contractile kinetics, via
962 Ca^{2+} dynamics and ATP production. Together, these data describe a previously unknown
963 mechanism to regulate skeletal muscle dynamics. These data provide the foundation for a proposed
964 mechanism of TCAP-1 action in skeletal muscle. TCAP-1 interacts with LPHN-1 and -3 to
965 stimulate the activation of G-protein-coupled PLC leading to the increased conversion of PIP3 into
966 IP3 and DAG. Increased IP3 levels stimulates the IP3R on the SR, opening Ca^{2+} channels to
967 increase cytosolic Ca^{2+} levels. Cytosolic Ca^{2+} is imported into the mitochondria likely via the Ca^{2+}
968 uniporter (MCU) which stimulates the TCA cycle and electron transport chain (ETC). Enhanced
969 ETC activity results in increased proton extrusion from the mitochondrial matrix and
970 hyperpolarization of mitochondrial membrane potential. This ultimately results in increased ATP
971 and NADH production, as well as increased SDH-ATP levels. Ca^{2+} is subsequently pumped out
972 of the mitochondria likely via Na^{+}/Ca^{2+} exchangers (NCX), thus restoring homeostatic levels of
973 Ca^{2+}. Moreover, we showed that the TCAP-1 increased cellular energy availability by increased
974 glucose importation into cells likely due to increased GLUT4 expression. The TCAP-1 mediated
975 mechanism is likely due to its interactions with LPHNs -1 and -3.

976

977 # Acknowledgments

978 We thank the Canadian Natural Sciences and Engineering Research Council (NSERC) for
979 Discovery Grants to Profs. D.A. Lovejoy, M. Locke and L. Buck and for NSERC Post-Graduate
980 Scholarships to Dr. Andrea Reid, Yani Chen, Mei Xu and Mia Husic and an Ontario Graduate
981 Scholarship to Thomas Dodsworth. We also thank Protagenic Therapeutics Inc. for operational
982 funding to Prof. D.A. Lovejoy

983

984 ***Author Contributions:***

985 Dr. Andrea Reid performed most of the experiments in this study, and wrote the initial draft of this
986 paper. Dr. David Hogg developed many of the calcium-associated experiments and supervised the
987 calcium studies and analyses, Dr. D. Barsyte and T. Dodsworth developed the strategy, preparation
988 and analyses of the siRNA and CRISPR cell lines. Prof. P. Biga and R. Reid provided the guidance
989 on the role of TCAP with respect to mitochondrial respirations and NADH assays, Dr. A. Slee
990 provided critical information on TCAP-1 kinetics. Prof. L. Buck provided the guidance for the
991 studies on energy metabolism in cells, and Prof. M. Locke developed and supervised the *in vivo*
992 studies on muscle metabolism. Mei Xu designed and performed the initial experiments to
993 determine the energy actions of TCAP in cells, Yani Chen developed the methods and analysed
994 the uptake of glucose in muscle cells in *in vivo* and *in vitro*. Mia Husic established some of the
995 methods for the cell culture of the transgenic cells and Prof. D. Lovejoy oversaw the entire research
996 program and analyses, and prepared the final drafts of the manuscript.

997

References

1. Ni T, Yue J, Sun G, Zou Y, Wen J, Huang J. Ancient gene transfer from algae to animals: mechanisms and evolutionary significance. BMC Mol Biol 2012; 12: 83.

2. Ramulu HG, Raoult D, Pontarotti P. The rhizome of life: what about metazoans? Cell Infect Microbiol. 2012; 2: 1–11.

3. Lovejoy DA, Hogg DW. Information processing in affective disorders: Did an ancient peptide regulating intercellular metabolism become co-opted for noxious stress sensing? BioEssays 2020; 2000039: 1-8.

4. Chand D, De Lannoy L, Tucker RP, Lovejoy DA. Origin of chordate peptides by horizontal protozoan gene transfer in early metazoans and protists: Evolution of the teneurin C-terminal associated peptides. Gen Comp Endocrinol 2013; 188: 144-150.

5. King N, Hittinger CT, Carroll SB. Evolution of key cell signaling and adhesion protein families predates animal origins. Science 2003; 301: 361–363.

6. King N, Westbrook MJ, Young SL, Kuo A, Abedin M, Chapman J. et al. The genome of the choanoflagellate Monosiga brevicollis and the origin of metazoans. Nature 2008; 451: 783–788.

7. Strotmann R, Schrock K, Boselt I, Staubert C, Russ A, Schoneberg T. Evolution of GPCR: Change and continuity. Mol Cell Endocrinol. 2011; 331: 170-178.

8. Tucker RP. Horizontal gene transfer in choanoflagellates. J Exp Zool B Mol Dev Evol 2013; 320: 1–9.

9. Zhang D, de Souza RF, Anantharaman V, Iyer LM, Aravind L. Polymorphic toxin systems: comprehensive characterization of trafficking modes, mechanism of action, immunity and ecology using comparative genomics. Biol Direct. 2012; 7:18.

10. Baumgartner S, Martin D, Hagios C, Chiquet-Ehrismann R. Ten-m, a Drosophilia gene related to tenascin is a new pair-rule gene. EMBO J. 1994; 13: 3728-3740.

11. Hong W, Mosca TJ, Luo L. Teneurins instruct synaptic partner matching in an olfactory map. Nature 2012; 484: 201–207.

12. Kenzelmann D, Chiquet-Ehrismann R, Leachman NT, Tucker RP. Teneurin-1 is expressed in interconnected regions of the developing brain and is processed in vivo. BMC Dev Biol. 2008; 8: 30.

13. Levine A, Bashan-Ahrend A, Budai-Hadrian O, Gartenber D, Menasherow S, Wides R. Odd Oz: a novel Drosophila pair-rule gene. Cell 1994; 77: 587-598.

14. Li J, Shalev-Benami M, Sando R, Jiang X, Kibrom A, Wang J. et al. Structural basis for teneurin function in circuit-wiring: a toxin motif at the synapse. Cell 2018; 173: 735-748.

15. Mosca TJ, Hong W, Dani VS, Favaloro V, Luo L. Trans-synaptic Teneurin signalling in neuromuscular synapse organization and target choice. Nature 2012; 484: 237-241.

16. Rubin BP, Tucker RP, Martin D, Chiquet-Ehrismann, R. Teneurins: a novel family of neuronal cell surface proteins invertebrates, homologous to the Drosophila pair-rule gene product Ten-m. Dev Biol 1999; 216: 195-209.

17. Tucker RP, Chiquet-Ehrismann R. Teneurins: a conserved family of transmembrane proteins involved in intercellular signalling during development. Dev Biol 2006; 290: 237-245.

18. Young TR, Leamey CA. Teneurins: important regulators of neural circuitry. Int J Biochem Cell Biol 2009; 41: 990–993.

19. Minet AD, Chiquet-Ehrismann R. Phylogenetic analysis of teneurin genes and comparison to the rearrangement hotspot elements of E. coli. Gene 2000; 257: 87–97.

1043 20. Minet AD, Rubin BP, Tucker RP, Baumgartner S. Chiquet-Ehrismann R. Teneurin-1, a
1044 vertebrate homologue of the Drosophila pair-rule gene ten-m, is a neuronal protein with a novel
1045 type of heparin-binding domain. J Cell Sci 1999; 112: 2019-2032.
1046 21. Oohashi T, Zhou XH, Feng K, Richter B, Mörgelin M, Perez MT, et al. Mouse ten-m/Odz is
1047 a new family of dimeric type II transmembrane proteins expressed in many tissues. Cell Biol
1048 1999; 145: 563-577.
1049 22. Jackson VA, Meijer DH, Carrasquero M, van Bezouwen LS, Lowe ED, Kleanthous C, et al.
1050 Structures of Teneurin adhesion receptors reveal an ancient fold for cell-cell interaction. Nat
1051 Commun 2018; 9:1079.
1052 23. Lovejoy DA, Al Chawaf A, Cadinouche A. Teneurin C-terminal associated peptides: An
1053 enigmatic family of neuropeptides with structural similarity to the corticotrophin releasing factor
1054 and calcitonin family of peptides. Gen Comp Endocrinol 2006; 148: 299-305.
1055 24. Wang L, Rotzinger S, Barsyte-Lovejoy D, Qian X, Elias CF, Bittencourt JC et al. Teneurin
1056 proteins possess a carboxy terminal corticotropin-releasing factor-like sequence that modulates
1057 emotionality and neuronal growth. Mol Brain Res 2005; 133: 253-265.
1058 25. Aravind L, Anantharaman V, Zhang D, de Sousa RF, Iyer LM. Gene flow and biological
1059 conflict systems in the evolution of eukaryotes. Front Cell Infect Microbiol 2012; 2: 89.
1060 26. Michalec OM, Chang B, Lovejoy N, Lovejoy DA. Corticotropin-releasing factor (CRF) and
1061 its relationship to an ancient peptide family. Front Endocrinol 2020; 11: 529.
1062 27. Sekar R, Chow BKC. Role of the secretin peptide family and their receptors in the
1063 hypothalamic control of energy homeostasis. Horm Metab Res 2013; 45:945-954.
1064 28. Araç D, Li J. Teneurins and latrophilins: two giants meet at the synapse. Curr Opin Struct
1065 Biol 2019; 54: 141-151.

1066 29. Fredricksson R, Lagerstrom L, Lundin LG, Schioth H. The G protein coupled receptors in the
1067 human genome form five main families. Phylogenetic analysis, paralogon groups and fingerprints.
1068 Mol. Pharmacol. 2003; 63: 1256-1272.
1069 30. Fredriksson R, Schiöth H, The repertoire of G-protein coupled receptors in fully sequenced
1070 genomes. Mol Pharmacol 2005; 67: 1414-1425.
1071 31. Silva JP, Lelianova VG, Ermolyuk YS, Vysokov N, Hitchen PG, Berninghausen O et al.
1072 Latrophilin 1 and its endogenous ligand Lasso/teneurin-2 form a high-affinity trans-synaptic
1073 receptor pair with signaling capabilities. Proc Natl Acad Sci USA 2011; 108: 12113-12118.
1074 32. Husic M, Barsyte-Lovejoy D, Lovejoy DA. Teneurin C-terminal associated peptide (TCAP)-
1075 1 and latrophilin interaction in HEK293 cells: Evidence for modulation for intercellular adhesion.
1076 Front. Endocrinol. 2019; 10: 22.
1077 33. Chand D, Casatti CA, DeLannoy L, Song L, Kollara A, Barsyte-Lovejoy D, et al. C-terminal
1078 processing of the teneurin proteins: Independent actions of a teneurin C-terminal associated
1079 peptide in hippocampal cells. Mol Cell Neurosci. 2013; 52: 38-50.
1080 34. Reid RM, Reid AL, Lovejoy DA, Biga PR. Teneurin C-terminal associated peptide (TCAP)-3
1081 increases metabolic activity in zebrafish. Front Mar Sci. 2021; 7: 591160.
1082 35. Tan L, Xu K, Vaccarino F, Lovejoy DA, Rotzinger S. Repeated intracerebral teneurin C-
1083 terminal associated peptide (TCAP)-1 injections produce enduring changes in behavioral
1084 responses to corticotropin-releasing factor (CRF) in rat models of anxiety. Behav Brain Res 2008;
1085 188, 195-200.
1086 36. Tan LA, Al Chawaf A, Vaccarino FJ, Boutros JC, Lovejoy DA. Teneurin C-terminal
1087 associated peptide (TCAP)-1 increases dendritic spine density in hippocampal neurons and
1088 decreases anxiety-like behaviors in rats. Physiol Behav 2011; 104: 199-204.

1089 37. Al Chawaf A, St. Amant K, Belsham DD, Lovejoy DA. Regulation of neurite outgrowth in
1090 immortalized hypothalamic cells and hippocampal primary cultures by teneurin C-terminal
1091 associate peptide-1 (TCAP-1). Neuroscience 2007; 144: 1241-1254.
1092 38. Chand D, Song L, De Lannoy L, Barsyte-Lovejoy D, Ackloo S, Boutros PC et al. C-terminal
1093 region of teneurin-1 co-localizes with dystroglycan and modulates cytoskeletal organization
1094 through an ERK-dependent stathmin- and filamin A-mediated mechanism in hippocampal cells.
1095 Neuroscience 2012; 219: 255-270.
1096 39. Hogg DW, Chen Y, D'Aquila AL, Xu M, Husic M, Tan LA et al. A novel role of the
1097 corticotropin-releasing hormone (CRH) regulating peptide, teneurin C-terminal associated peptide
1098 (TCAP)-1 on glucose uptake into the brain. J Neuroendocrinol 2018; 30: e12579.
1099 40. Richter EA, Hargraves M. GLUT4 and skeletal muscle glucose uptake. Physiol Rev 2013; 93:
1100 993-1017.
1101 41. Santos JM, Ribeiro SB, Gaya AR, Appell HJ, Duarte JA. Skeletal muscle pathways of
1102 contraction-enhanced glucose uptake. Int J Sports Med 2008; 29: 785–794.
1103 42. Sayer AA, Dennison EM, Syddall HE, Gilbody HJ, Philips DIW, Cooper C. Type 2 diabetes,
1104 muscle strength, and impaired physical function: the tip of the iceberg? Diabetes Care 2005; 28:
1105 2541-2542.
1106 43. Holwerda AM, Locke M. Hsp25 and Hsp72 content in rat skeletal muscle following controlled
1107 shortening and lengthening contractions. Appl Physiol Nutr Met 2014; 39: 1380–1387.
1108 44. Maher F. Immunocolocalization of GLUT1 and GLUT3 glucose transporters in primary
1109 culture neurons and glial. J Neurosci Res 1995; 42: 459-469.
1110 45. Uemura E, Greenlee HW. Insulin regulates neuronal glucose uptake by promoting
1111 translocation of glucose transporter GLUT3. Exp Neurol 2006; 198: 48-53.

1112 46. Liang H, Ward WF. PGC-1α: a key regulator of energy metabolism. Adv Physiol Educ 2006;
1113 30:154-151.
1114 47. Davletov BA, Shamotienko OG, Lelianova VG, Grishin V, Ushkaryov YA. Isolation and
1115 biochemical characterization of a calcium-independent alpha-latrotoxin-binding protein. J Biol
1116 Chem 1996; 1271: 23239-23245.
1117 48. Silva J-P, Ushkaryov YA. The latrophilins, "split-personality" receptors. Adv Exp Med Biol
1118 2010; 706: 59-75.
1119 49. Qian X, Barsyte-Lovejoy D, Chewpoy RB, Wang L, Gautam N, Wang N et al. Characterization
1120 of teneurin C-terminal associated peptide (TCAP)-3 from rainbow trout hypothalamus. Gen Comp
1121 Endocrinol 2004; 137: 205-216.
1122 50. Al Chawaf A, Xu K, Tan L, Vaccarino F, Lovejoy DA, Rotzinger S. Corticotropin-releasing
1123 factor behaviours are modulated by intravenous administration of teneurin C-terminal associated
1124 peptides. Peptides 2007; 28: 1406-1415.
1125 51. Erb S, McPhee M, Brown ZJ, Kupferschmidt DA, Song L, Lovejoy DA. Repeated intravenous
1126 administrations of teneurin-C terminal associated peptide (TCAP)-1 attenuates reinstatement of
1127 cocaine seeking by corticotropin-releasing factor (CRF) in rats. Beh Brain Res 2014; 269: 1-5.
1128 52. Kupferschmidt D, Lovejoy DA, Rotzinger S, Erb S. Teneurin C-terminal associated peptide
1129 (TCAP)-1 blocks the effects of corticotropin-releasing factor (CRF) on the reinstatement of
1130 cocaine seeking and expression of cocaine-induced behavioral sensitization. Br J Pharmacol 2011;
1131 163: 574-583.
1132 53. Rotzinger, S, Lovejoy DA, Tan L. Behavioral effects of neuropeptide ligands in rodent models
1133 of depression and anxiety Peptides 2010; 31: 736-756.

1134 54. Tan LA, Chand D, De Almeida R, Xu M, Colacci M, De Lannoy et al. Modulation of
1135 neuroplastic changes and corticotropin-releasing factor associated behaviour by a phylogenetically
1136 ancient and conserved peptide family. Gen Comp Endocrinol 2012; 176: 309-313.
1137 55. Ishii K, Suzuki N, Mabuchi Y, Ito N, Kikura N, Fukada S-I et al. Muscle satellite cell protein
1138 teneurin-4 regulates differentiation during muscle regeneration. Stem Cells 2015; 33: 3017-3027.
1139 56. Calderón JC, Bolaños P, Caputo C. The excitation–contraction coupling mechanism in
1140 skeletal muscle Biophys Rev 2014; 6:133–160.
1141 57. Denton RM. Regulation of mitochondrial dehydrogenases by calcium ions. Biochim Biophys
1142 Acta 2009; 1787: 1309-1306.
1143 58. Wan B, La Noue KF, Cheung JY, Scaduto RC. Regulation of citric acid cycle by calcium. J
1144 Biol Chem 1989; 264:13430-13439.
1145 59. Dias-Vegas AR¸ Cardova A, Valladares D, Llanos P, Hildago C, Gharardi G et al.
1146 Mitochondrial calcium increase induced by RyR1 and IP_3R channel activation after membrane
1147 polarizations regulates skeletal muscle metabolism. Front Physiol 2018; 9: 791
1148 60. Rahman MA, Ashton AC, Meunier F, Davletov BA, Dolly JO, Ushkaryov YA. Norepinephrine
1149 exocytosis stimulated by alpha-latrotoxin requires both external and stored calcium, and is
1150 mediated by latrophilin, G proteins and phospholipase C. Phil Trans R Soc London B 1999; 354:
1151 379-386.
1152 61. J Lang , Y Ushkaryov, A Grasso, C B Wollheim. Ca2+-independent insulin exocytosis induced
1153 by alpha-latrotoxin requires latrophilin, a G protein-coupled receptor. EMBO J 1998; 17:648-57.
1154 62. Sando R, Südhof TC. Latrophilin GPCR signaling mediates synapse formation. Elife.
1155 2021;10:e65717.

1156 63. Rolfe DF, Brand MD. The physiological significance of mitochondrial proton leak in animal
1157 cells and tissues Biosci Rep 1997; 17: 9-16.
1158 64. Röthe J, Thor R, Winkler J, Knierim AB, Binder C, Huth S, et al. Involvement of the adhesion
1159 GPCRs latrophilin in the regulation of insulin release. Cell Rep 2019; 26: 1537-1584.
1160 65. Meza-Aguilar DG, Boucard AA. Latrophilins updated. Biomol Concepts 2014; 5: 457-478.
1161 66. Milligan G. Ward RJ, Marsango S. 2019 GPCR homo-oligomerization. Curr. Opin. Cell
1162 Biol. 57:40-47
1163 67. Volynski KA, Silva J-P, Lelianova VG, Atiqur Rahman M, Hopkins C, Ushkaryov YA.
1164 Latrophilin fragments behave as independent proteins that associate and signal on binding to
1165 LTX(N4C) EMBO J 2004: 23; 4423-4433.
1166 68 Müller A, Winkler J, Fiedler F, Sastraihardja T, Binder C, Schnabel R et al. Oriented cell
1167 division I the C. elegans embryo is coordinated by G-protein signaling dependent on the Adhesion
1168 GPCR LAT-1. PLOS Genetics 2015; 11: e1005624.
1169 69. Nazarko O, Kibrom A, Winkler J, Leon K, Stoveken H, Salzman G, et al. A comprehensive
1170 mutagenic screen of the Adhesion GPCR latrophin/ADGRL1. iScience 2015; 3; 264-278.
1171 70. Liebscher I, Schön J, Peterson SC, Fischer L, Auerback N, Demberg LM et al. A tethered
1172 agonist within the ectodomain activates the adhesion G protein-coupled receptors GPR126 and
1173 GPR133. Cell Rep 2014; 9: 2018-2026.
1174 71. Davletov BA, Meunier FA, Ashton AC, Matsushita H, Hirst WD, Lelianova VG, et al. Vesicle
1175 exocytosis stimulated by alpha-latrotoxin is mediated by latrophilin and requires both external and
1176 stored Ca2+. EMBO J 1998;17: 3909-3920.
1177 72. Lelianova VG, Davletov BA, Sterling A, Atiqur Rahman M, Grishin EV Totty NF et al. α-
1178 latrotoxin receptor, latrophilin, is a novel member of the secretin family of G protein-coupled

receptors. J. Biol. Chem. 1997; 272:21504-21521.

Figure 1

A

```
RAT TCAP-1              QQLLGTGRVQGYDGYFVLSVEQYLELSDSANNIHFMRQSEI-NH2
MOUSE TCAP-1            QQLLGTGRVQGYDGYFVLSVEQYLELSDSANNIHFMRQSEI-NH2

RAT TCAP-2              QQLLSTGRVQGYEGYYVLPVEQYPELADSSSNIQFLRQNEM-NH2
MOUSE TCAP-2            QQLLSTGRVQGYEGYYVLPVEQYPELADSSSNIQFLRQNEM-NH2

RAT TCAP-3              .QLLSAGKVQGYDGYYVLSVEQYPELADSANNIQFLRQSEI-NH2
MOUSE TCAP-3            .QLLSAGKVQGYDGYYVLSVEQYPELADSANNIQFLRQSEI-NH2

RAT TCAP-4              QQVLNTGRVQGYDGFFVTSVEQYPELSDSANNIHFMRQSEM-NH2
MOUSE TCAP-4            QQVLNTGRVQGYDGFFVTSVEQYPELSDSANNIHFMRQSEM-NH2
```


B

```
SYN. MOUSE TCAP-1       pEQLLGTGRVQGYDGYFVLSVEQYLELSDSANNIHFMRQSEI-NH2
SC.MOUSE TCAP-1         pETHSSLELRVSLIGEQQFIGYENQSDQNYGLLAYFDRVGMS-NH2
```

Figure 1

A

B

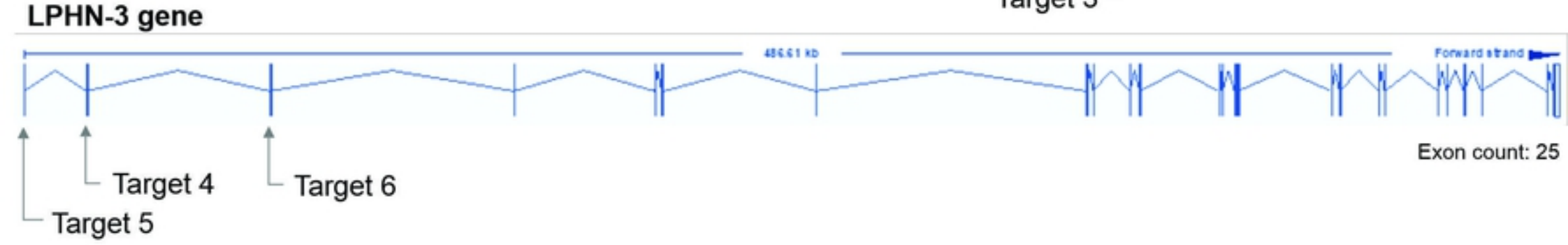

C

LPHN-1		LPHN-3	
Target 1	5'-ACATTGTCAAATATGACCTG-3'	Target 4	5'-GAGCGCTCAACGGCTCATCG-3'
Target 2	5'-TGGAACCTACAAATACCTGG-3'	Target 5	5'-CACGATGCTTTTAGCACCTG-3'
Target 3	5'-CGTGGACTATGCCTTCAACA-3'	Target 6	5'-TCGAGAGCGCCAACTACGGG-3'

Figure 2

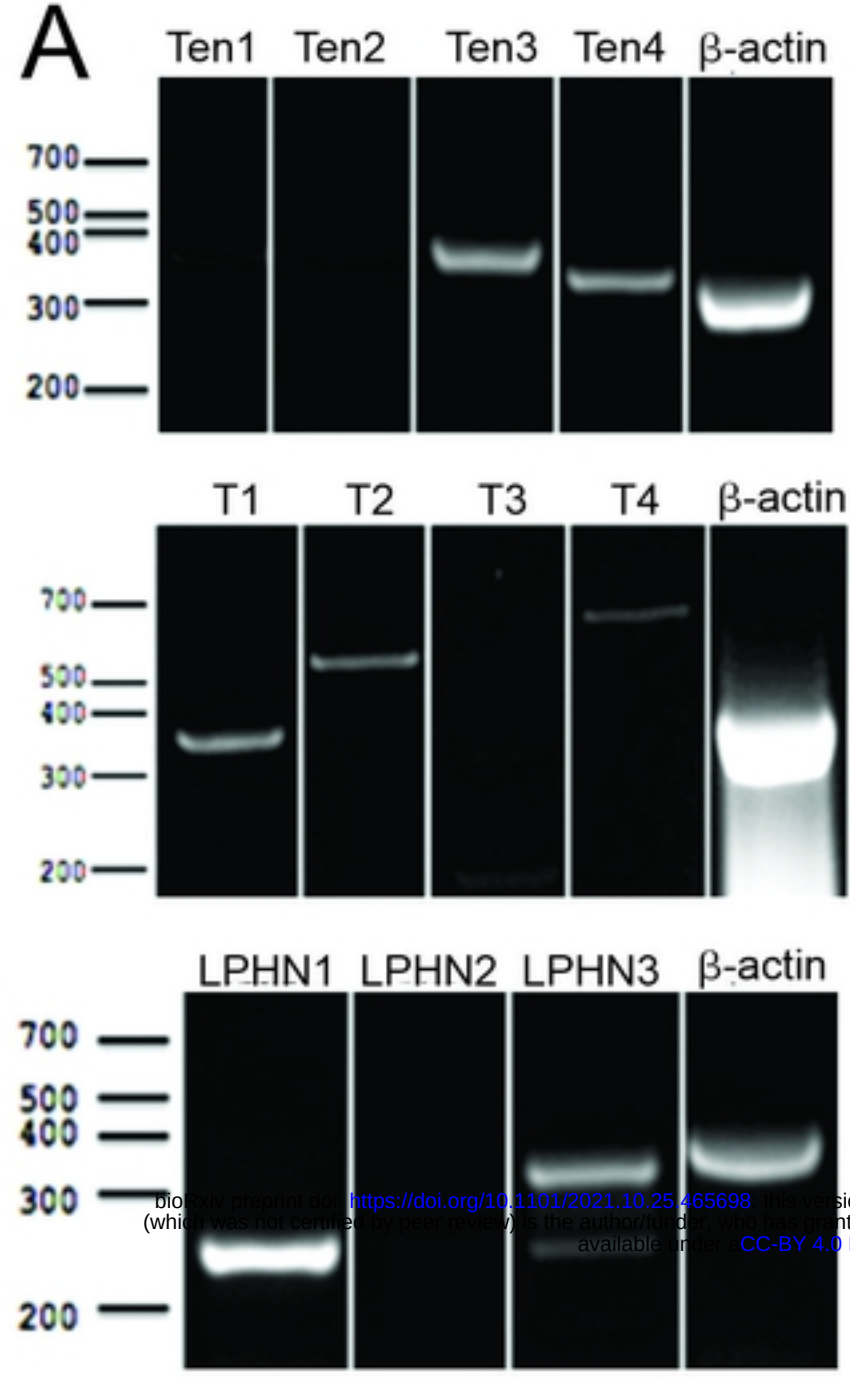

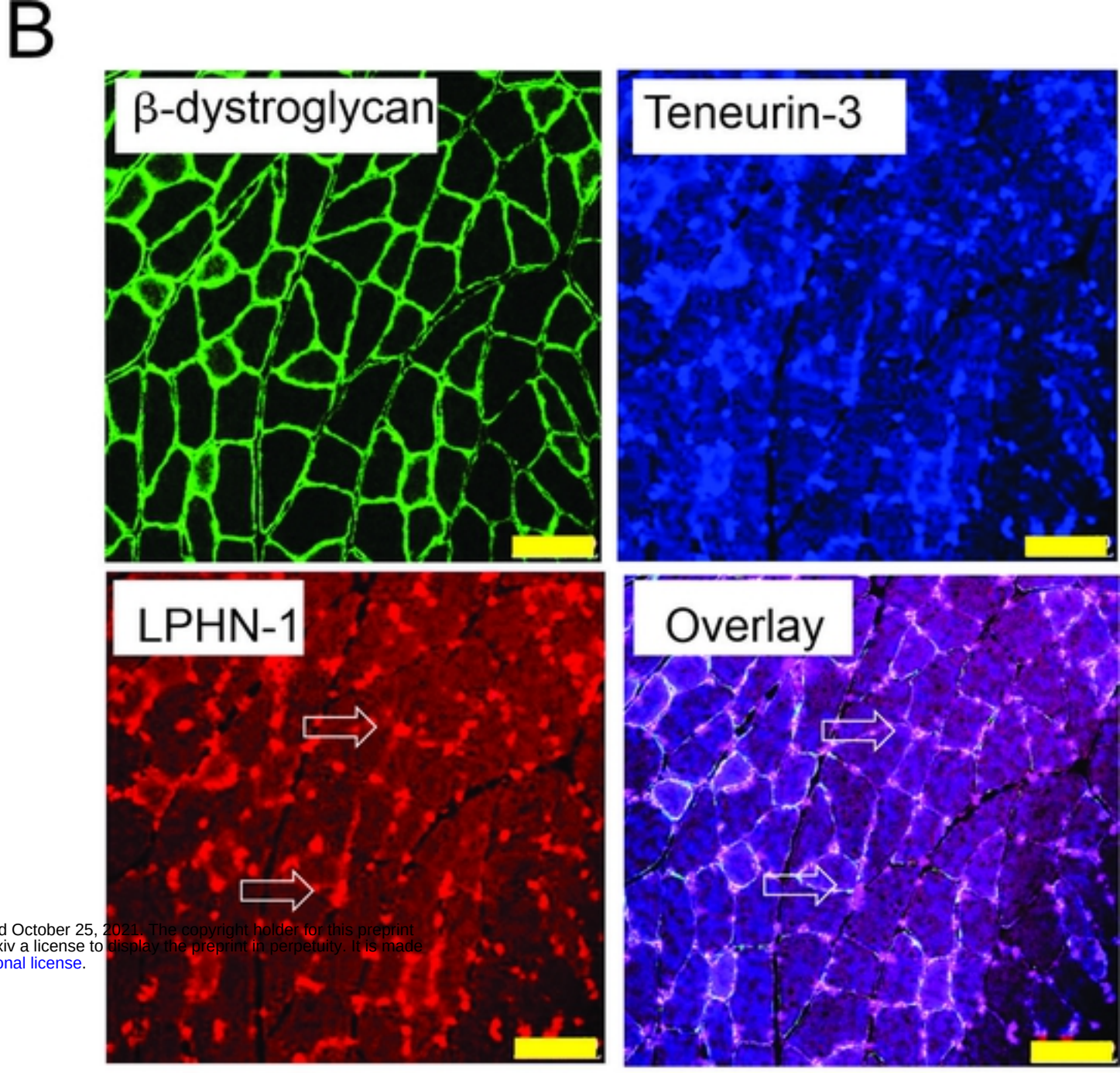

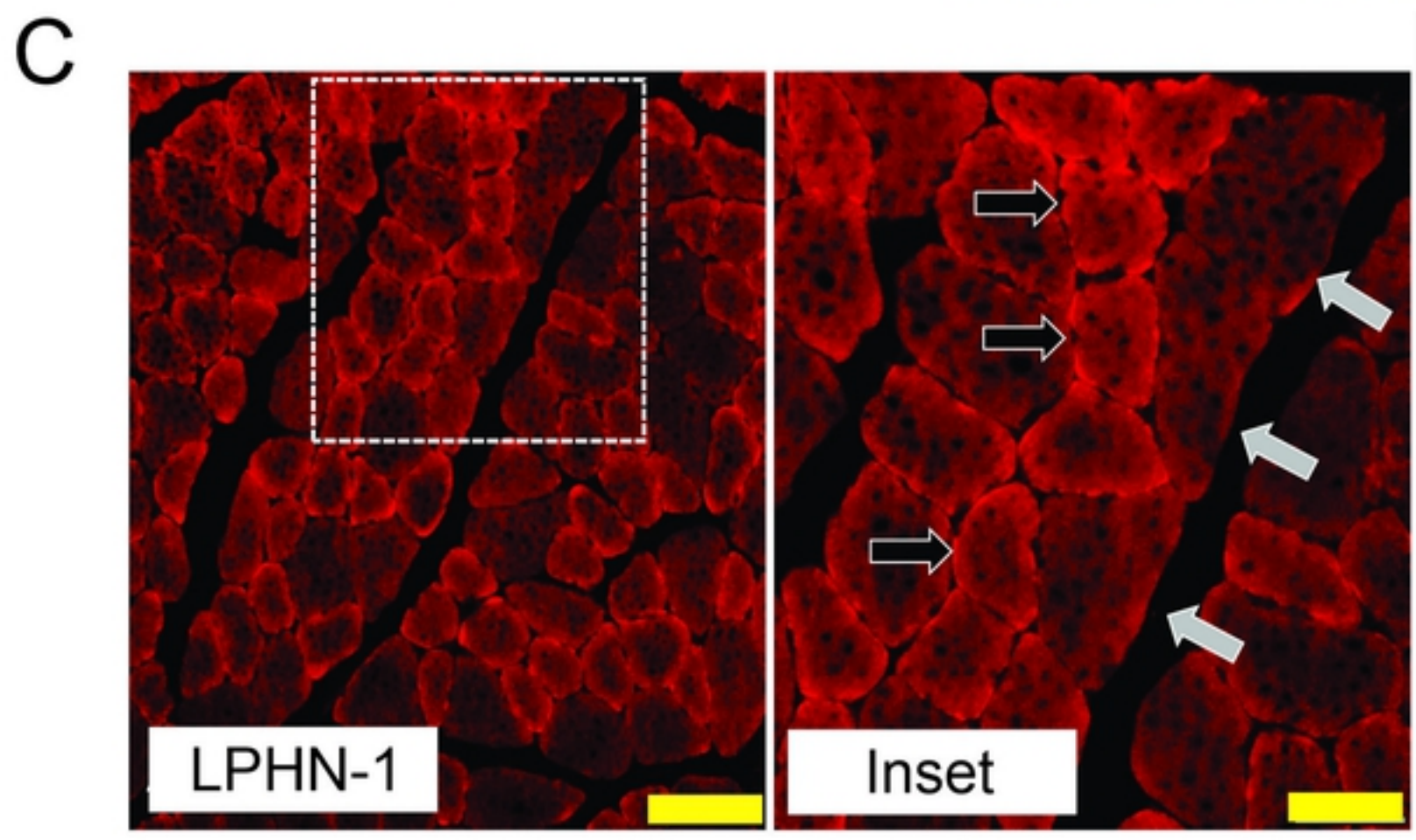

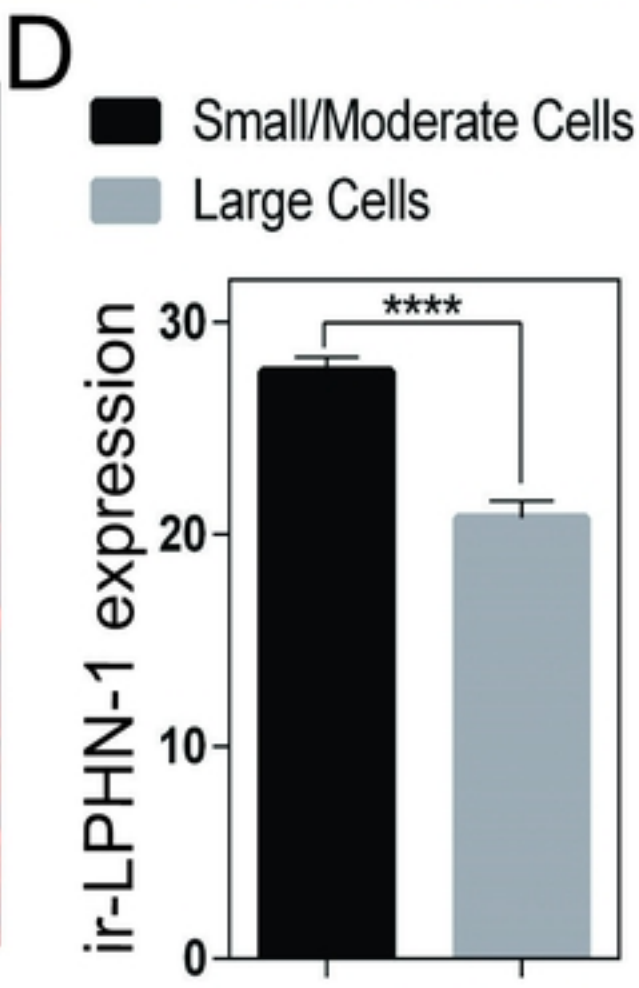

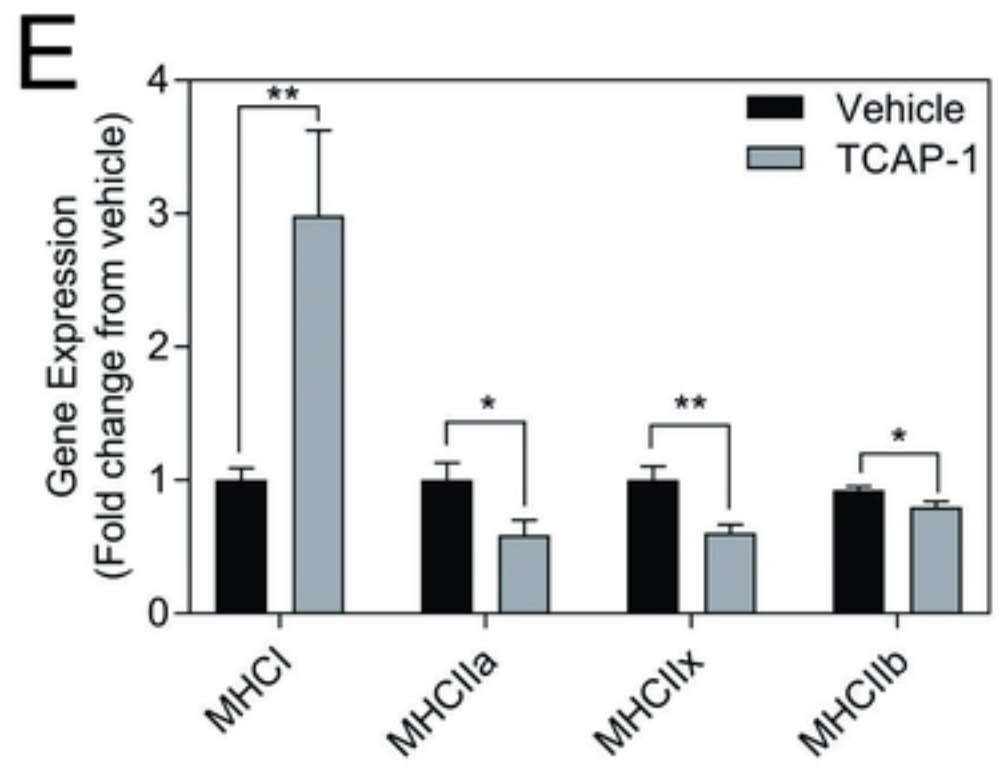

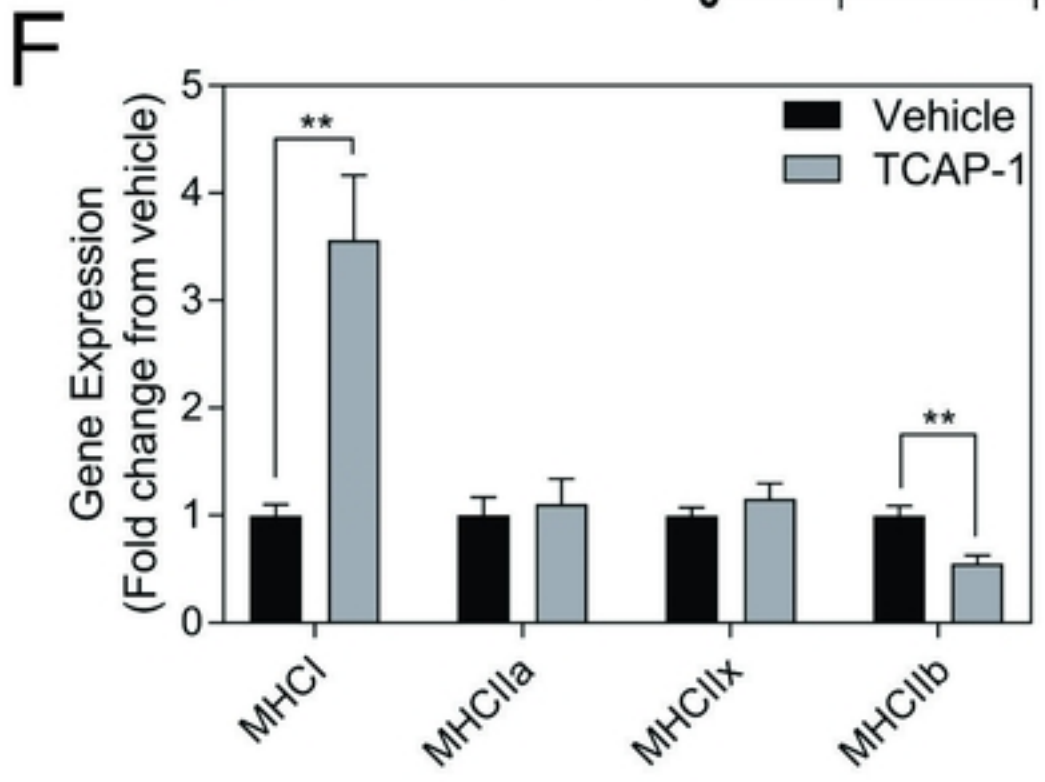

Figure 3

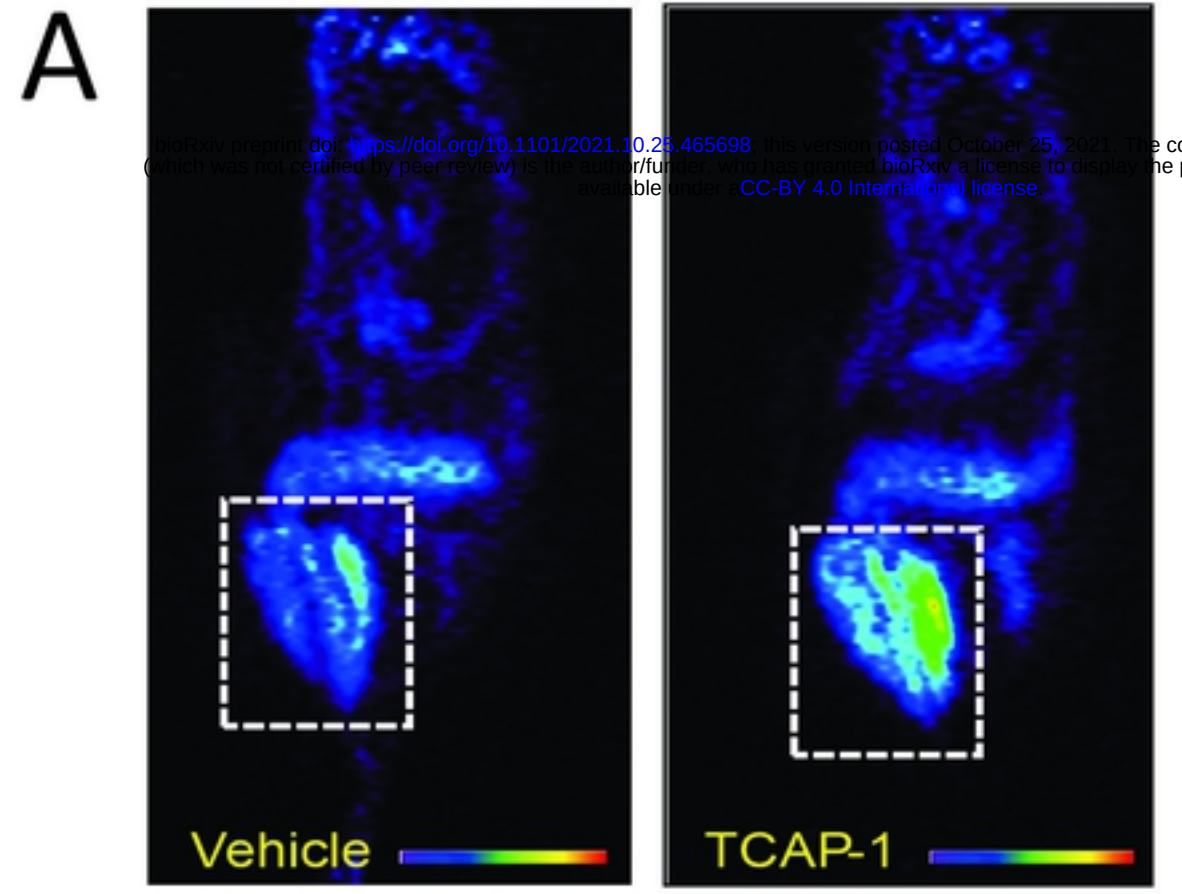

Figure 4

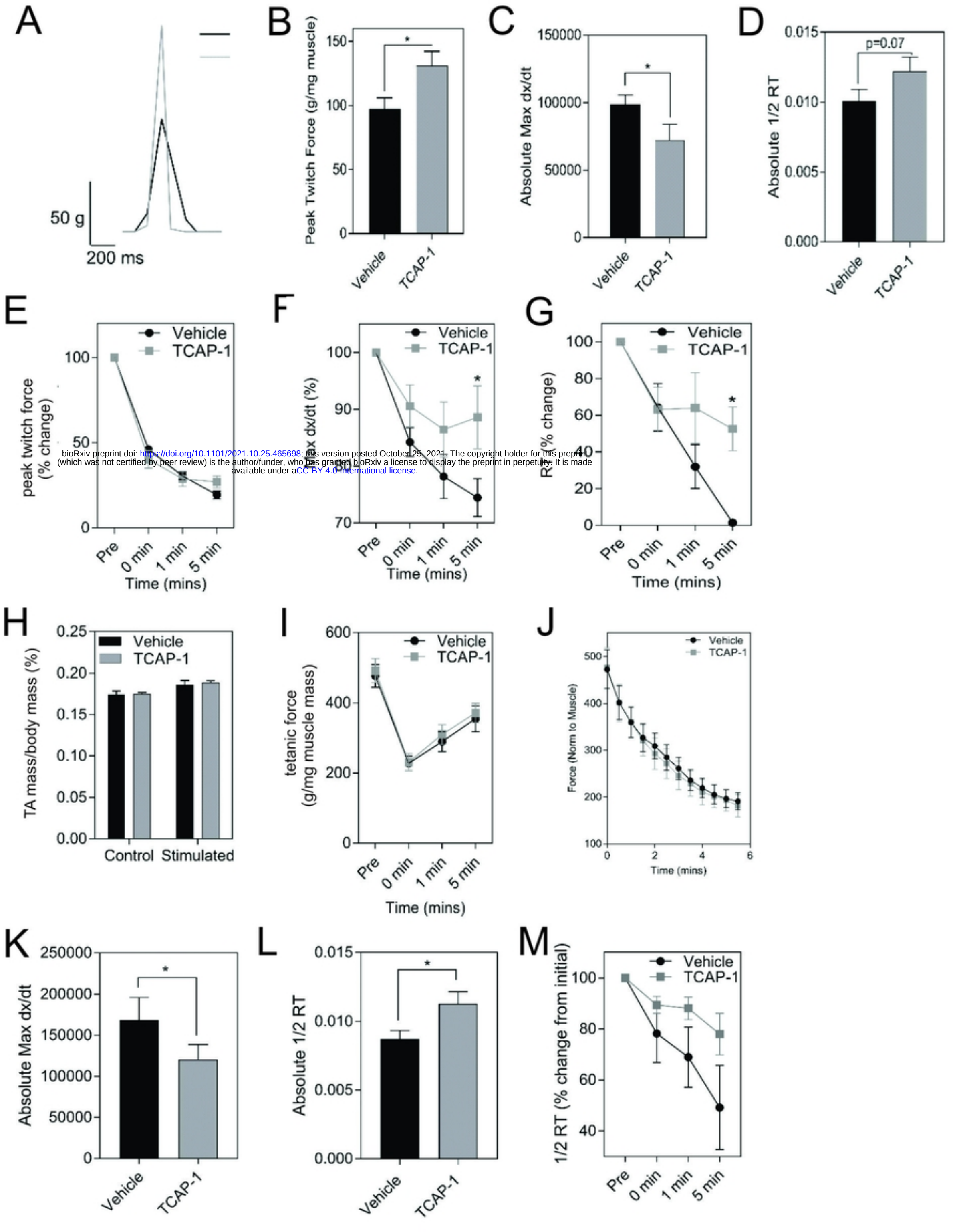

Figure 5

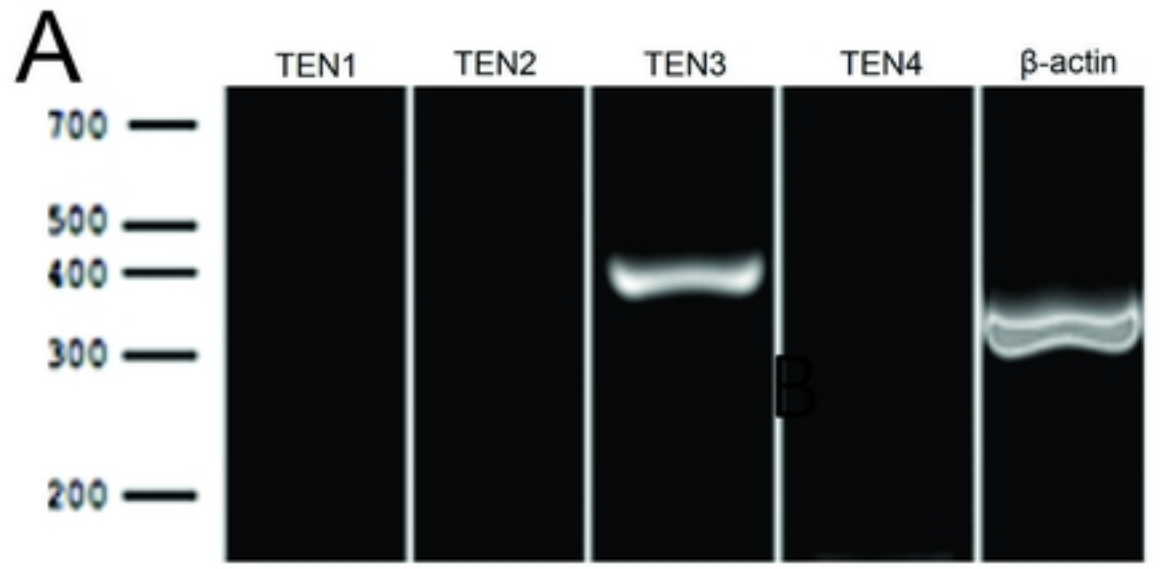

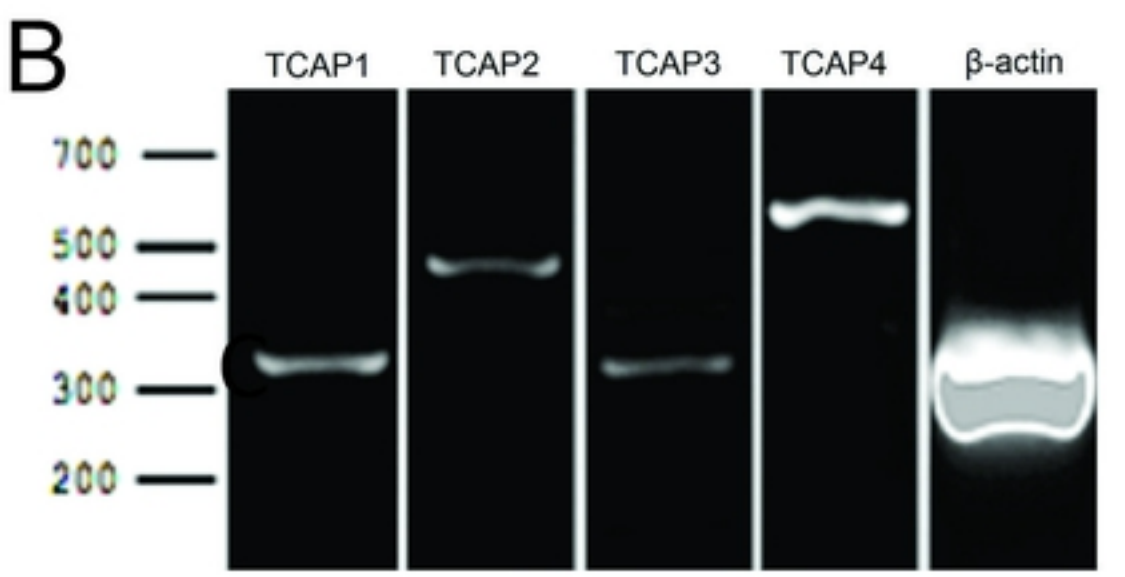

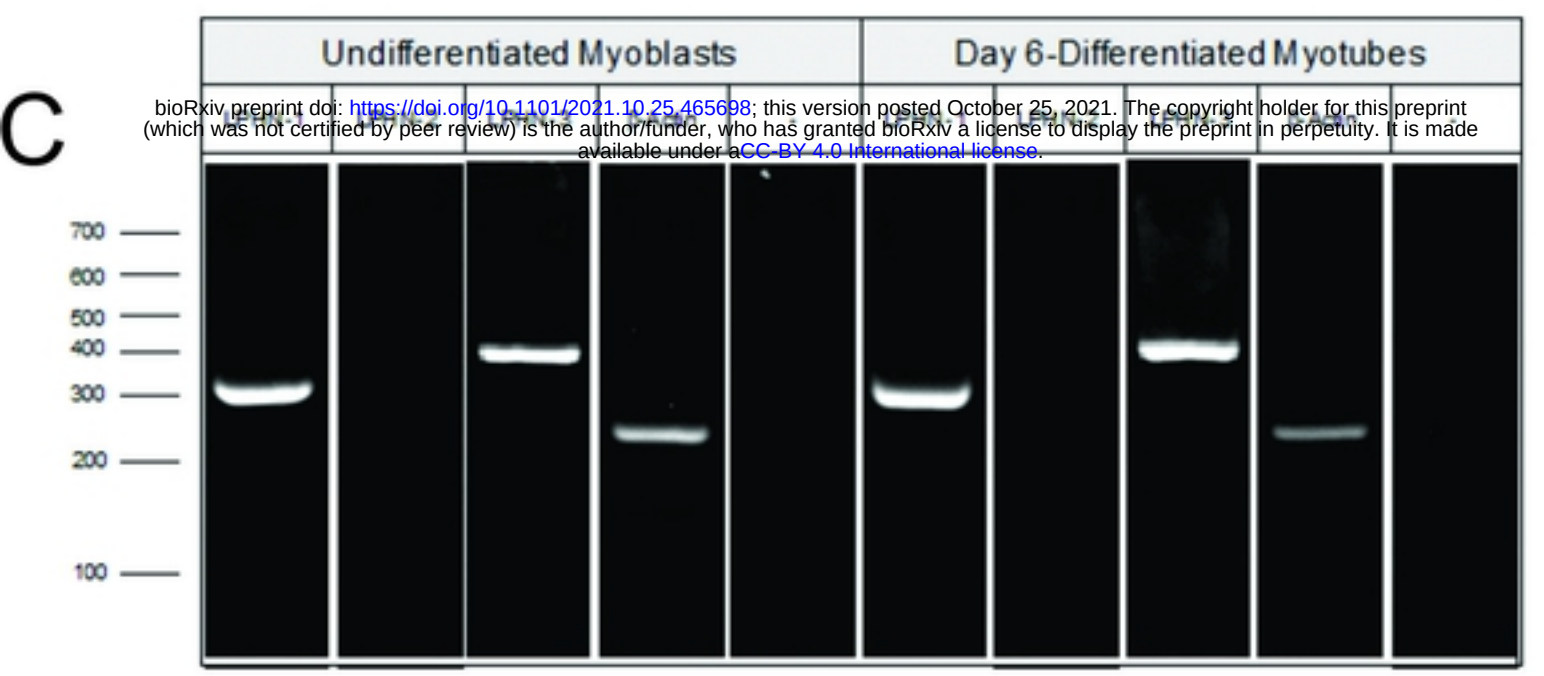

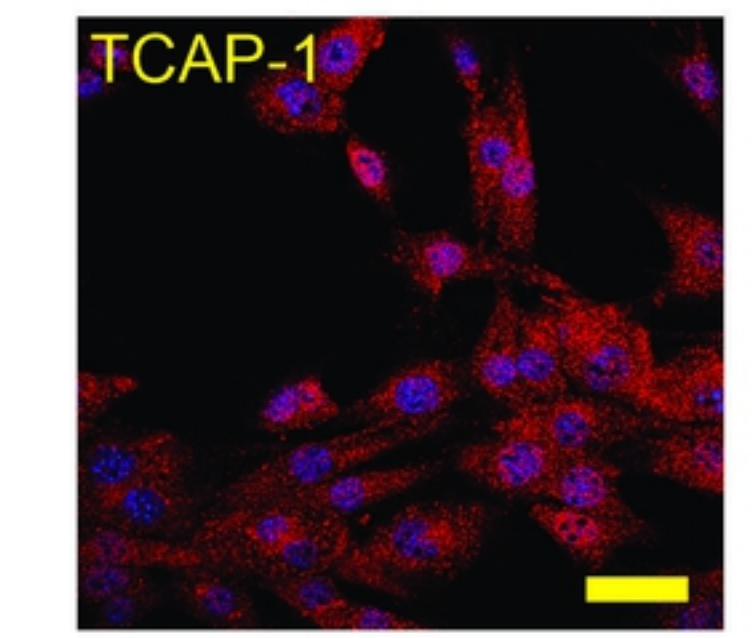

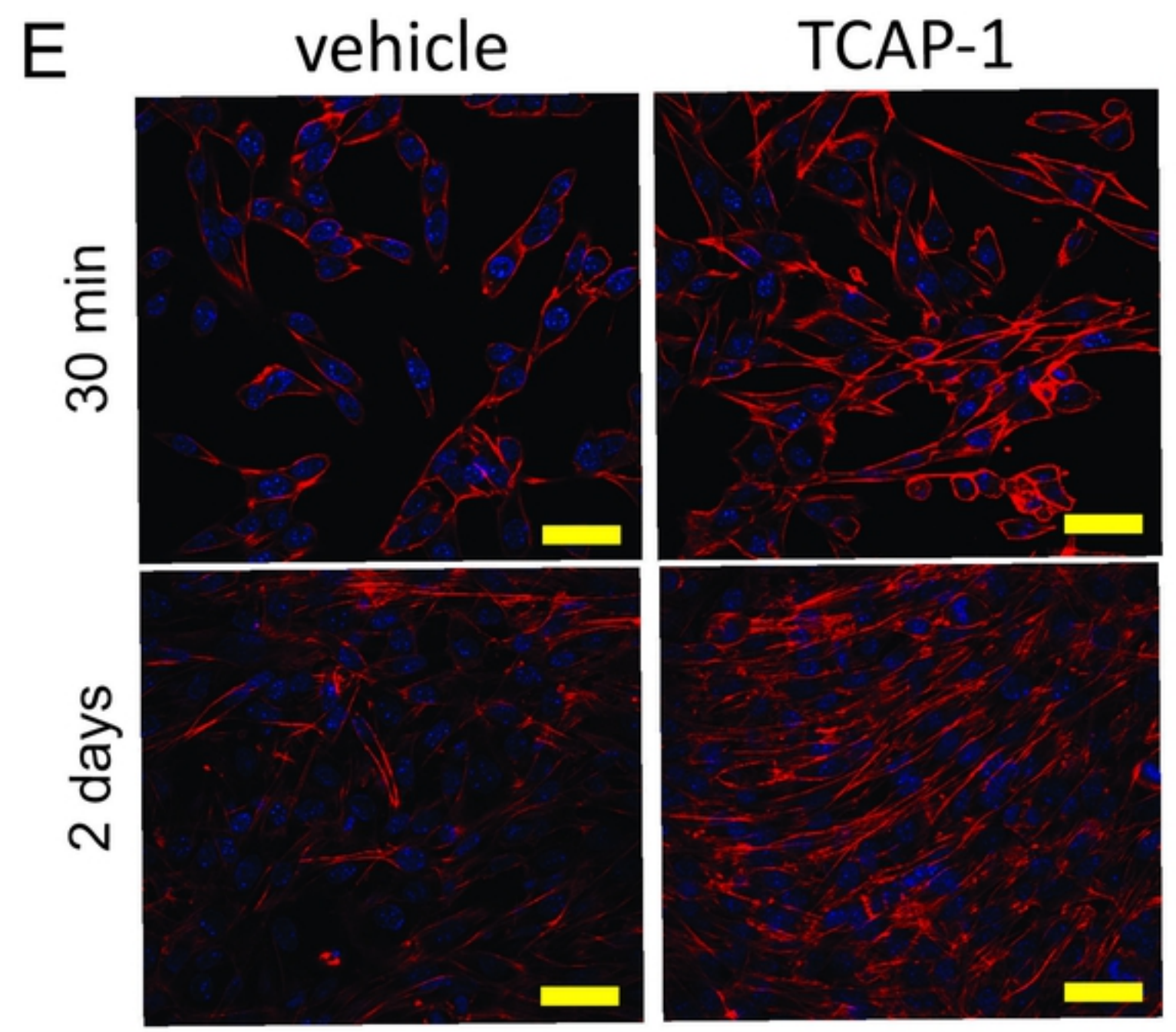

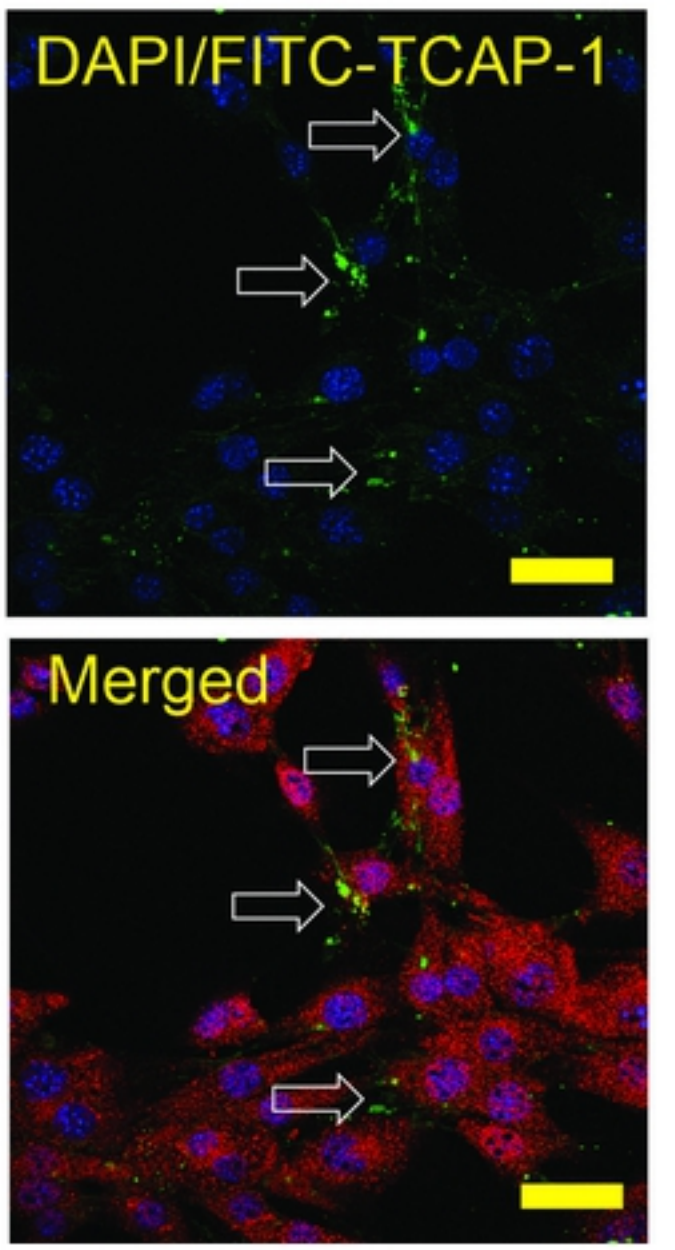

Figure 6

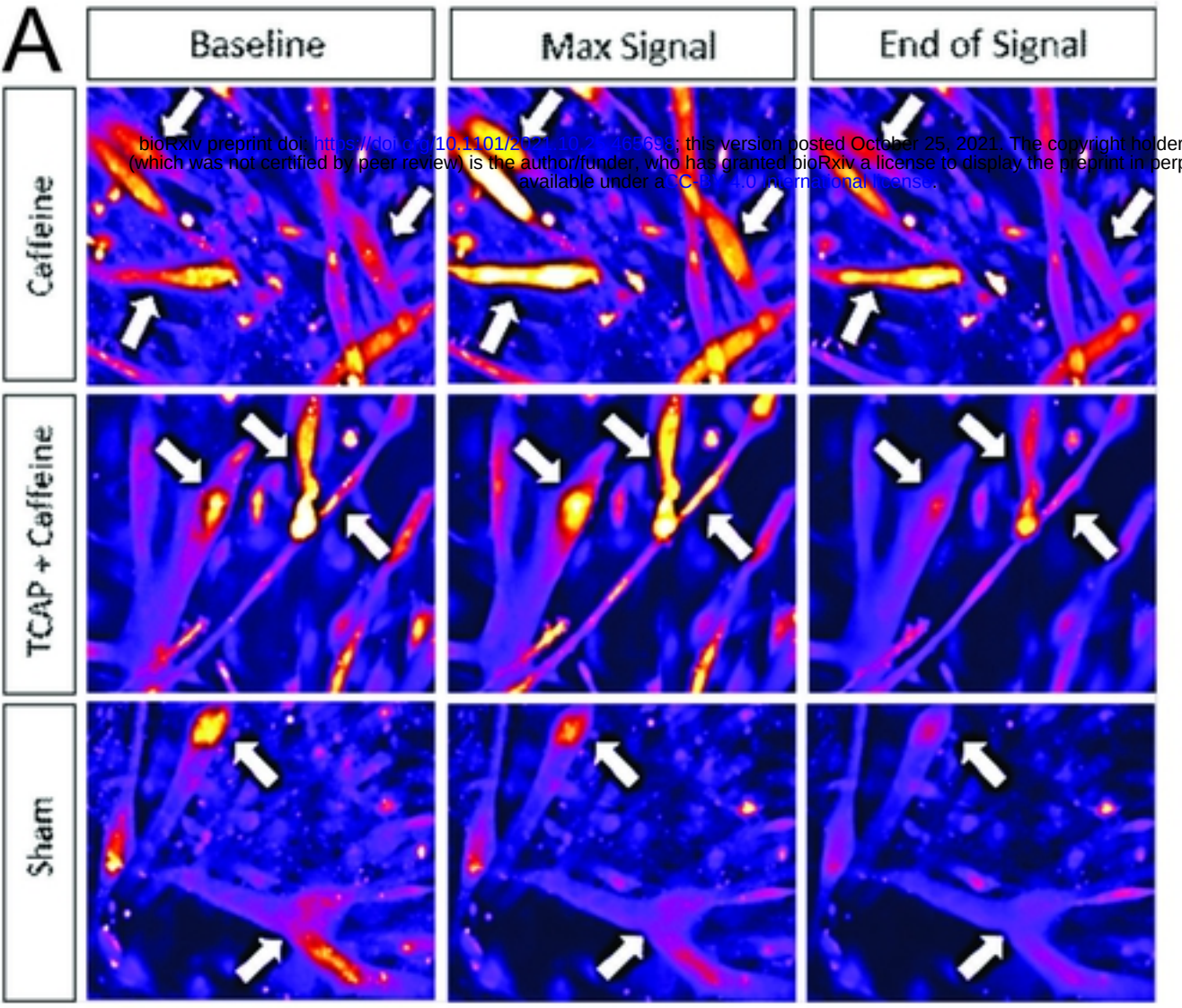

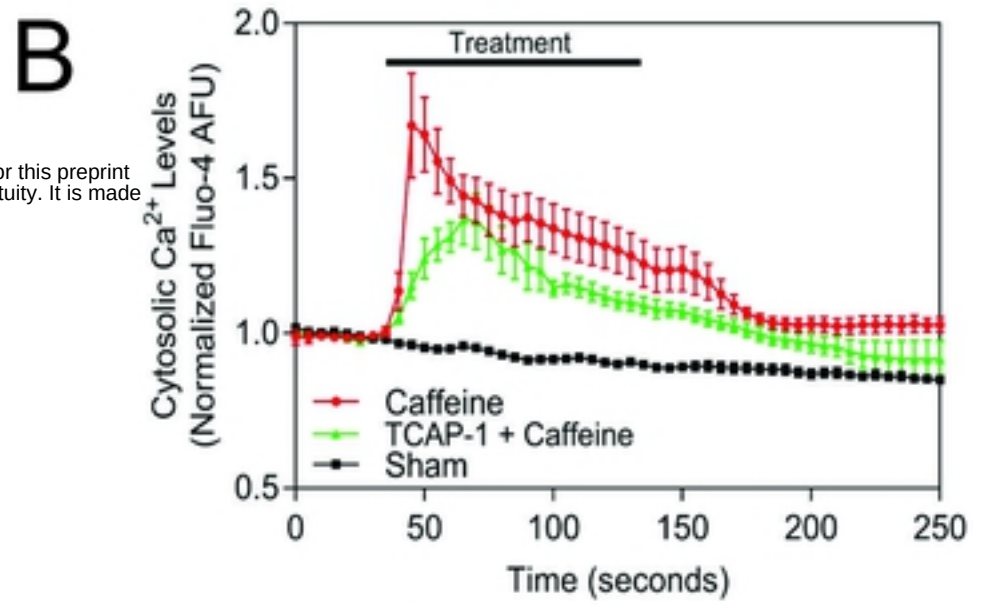

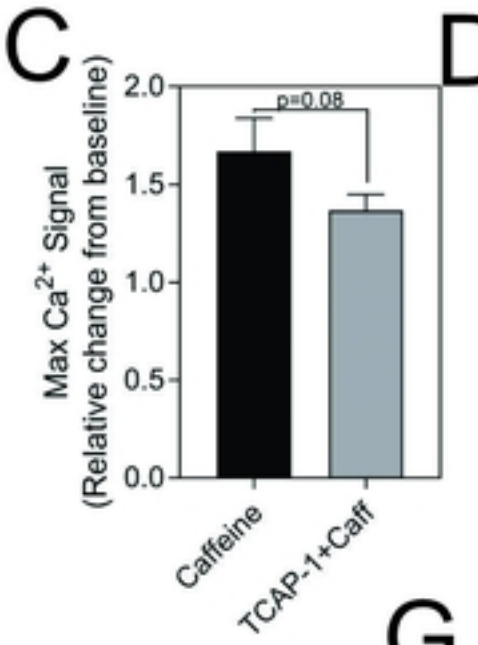

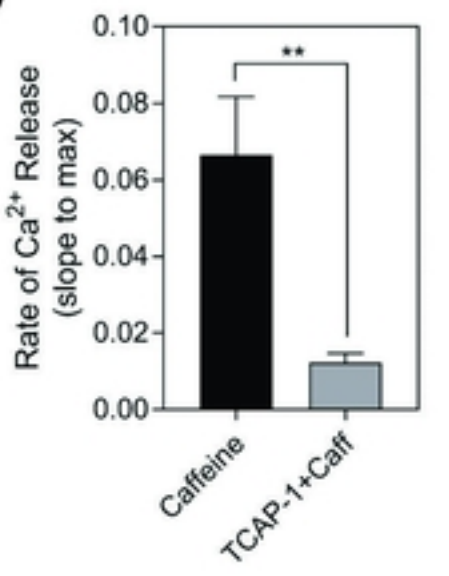

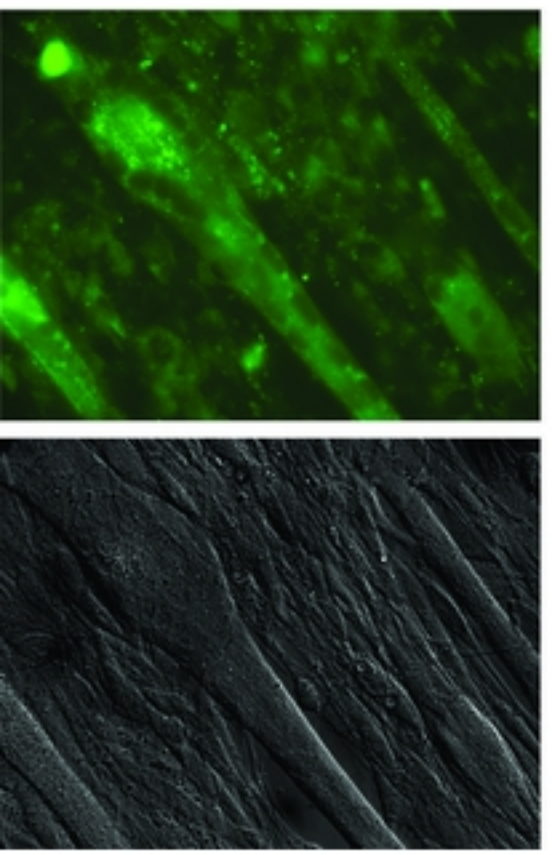

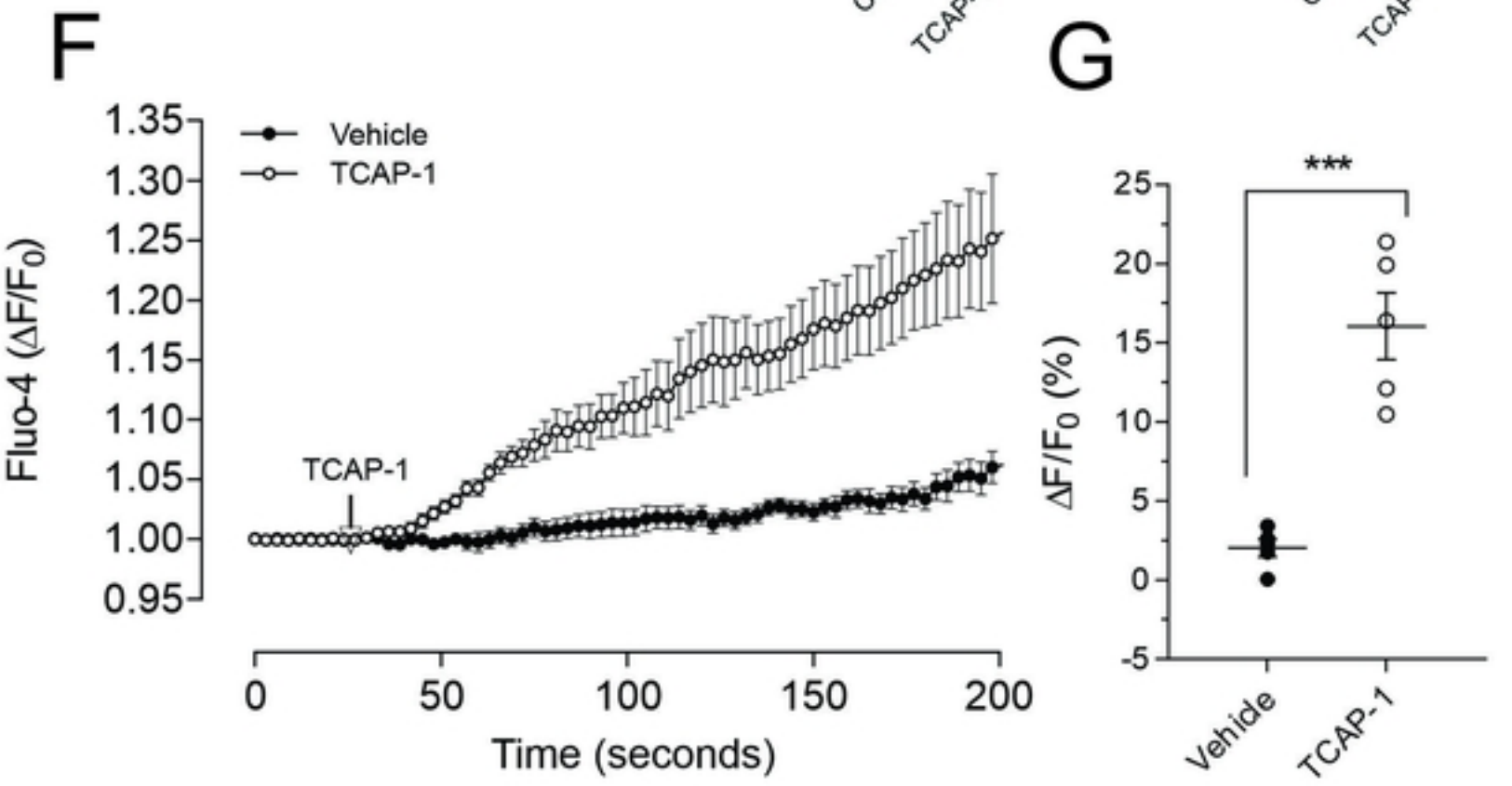

Figure 7

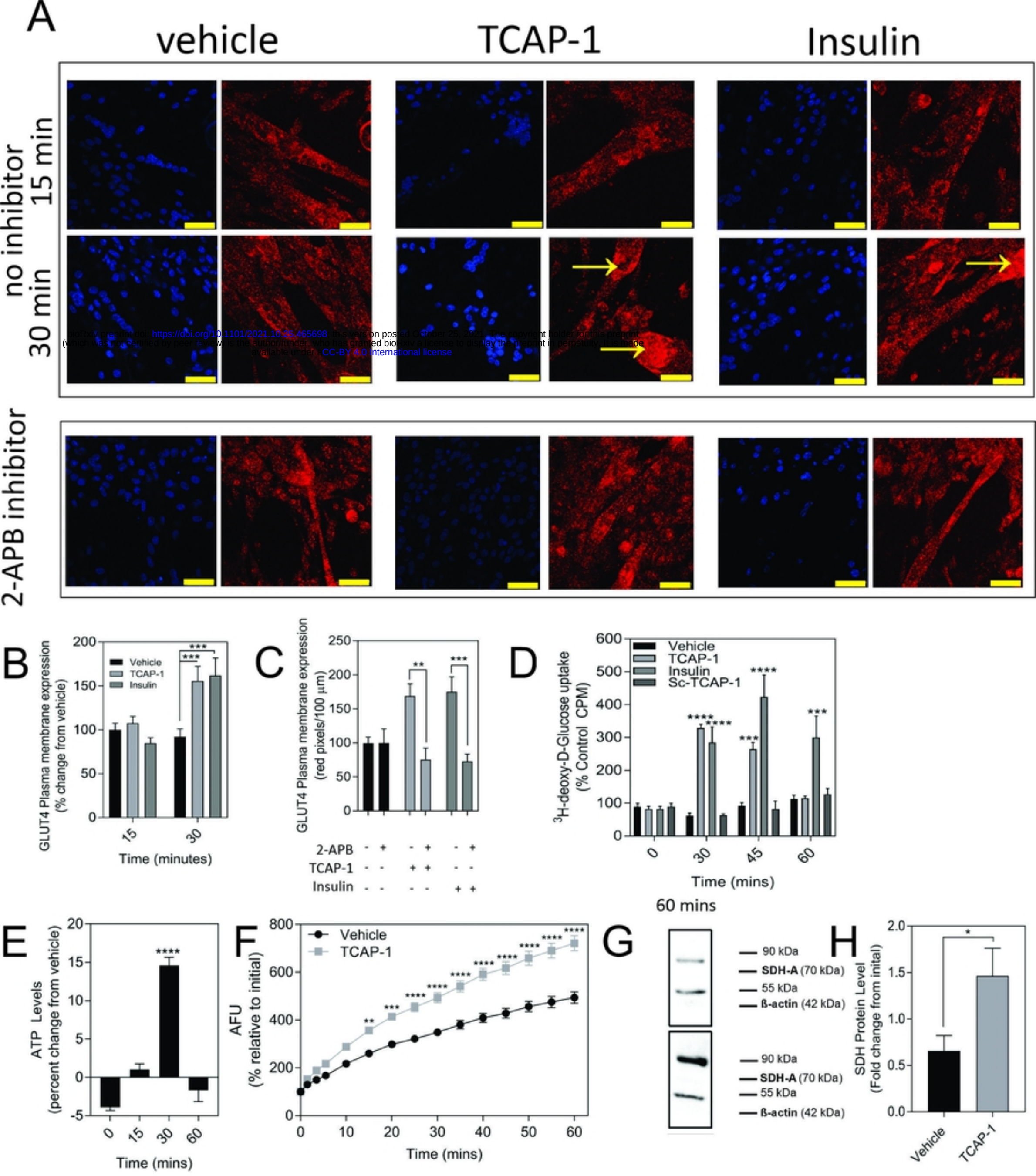

Figure 8

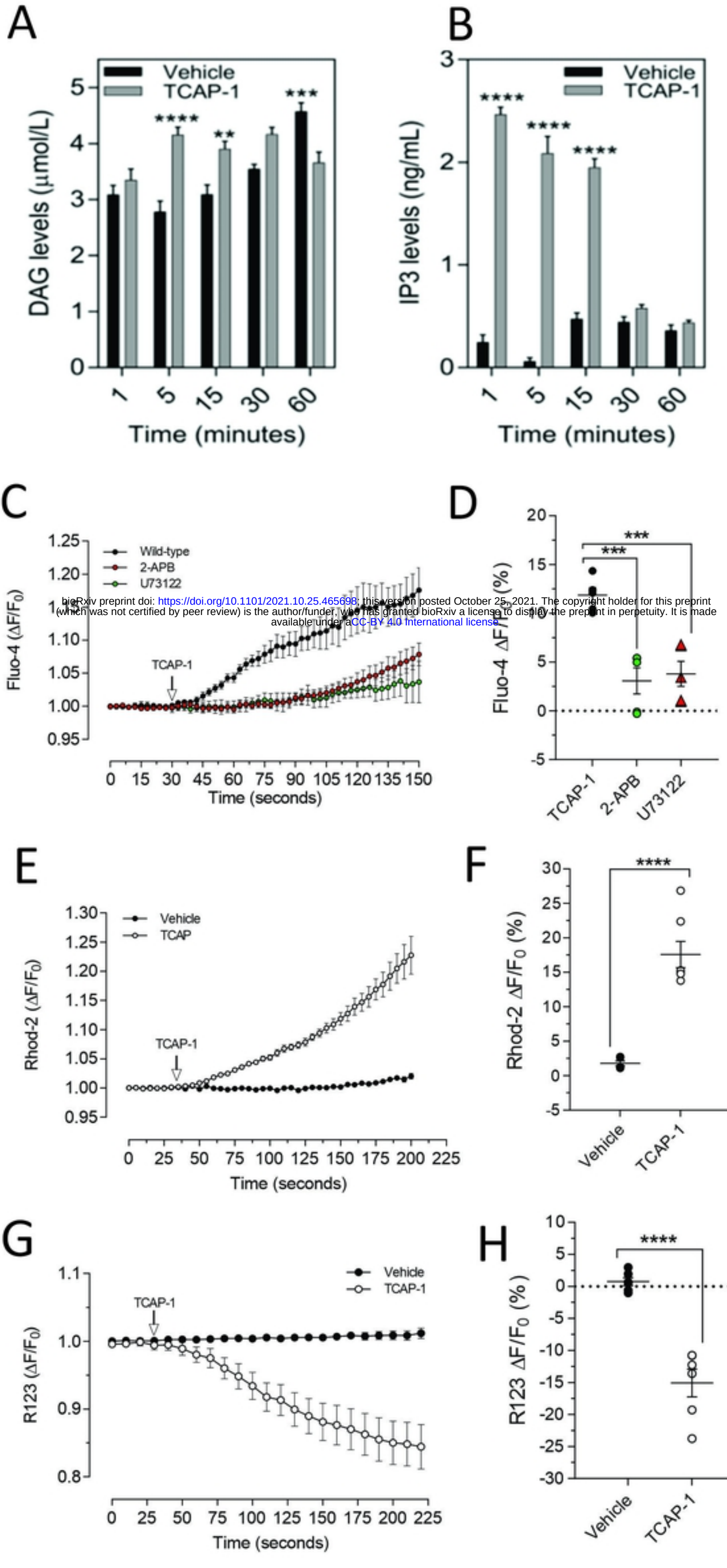

Figure 9

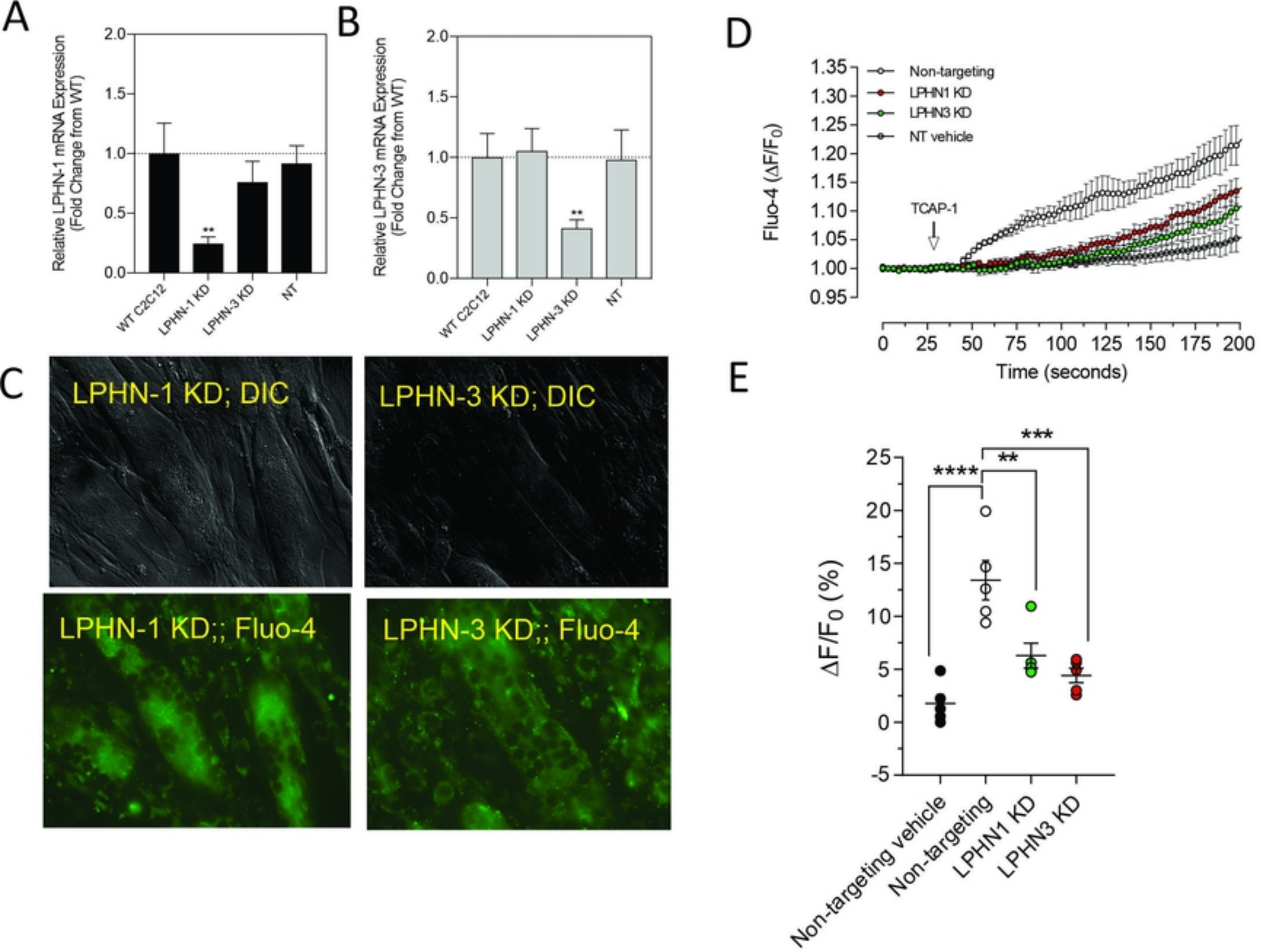
A
Relative LPHN-1 mRNA Expression (Fold Change from WT)
2.0
1.5
1.0
0.5
0.0
**
WT C2C12
LPHN-1 KD
LPHN-3 KD
NT
B
Relative LPHN-3 mRNA Expression (Fold Change from WT)
2.0
1.5
1.0
0.5
0.0
**
WT C2C12
LPHN-1 KD
LPHN-3 KD
NT
C
LPHN-1 KD; DIC
LPHN-3 KD; DIC
LPHN-1 KD;; Fluo-4
LPHN-3 KD;; Fluo-4
D
Fluo-4 (ΔF/F0)
1.35
1.30
1.25
1.20
1.15
1.10
1.05
1.00
0.95
Non-targeting
LPHN1 KD
LPHN3 KD
NT vehicle
TCAP-1
0
25
50
75
100
125
150
175
200
Time (seconds)
E
ΔF/F0 (%)
25
20
15
10
5
0
-5
****
**
***
Non-targeting vehicle
Non-targeting
LPHN1 KD
LPHN3 KD

Figure 10

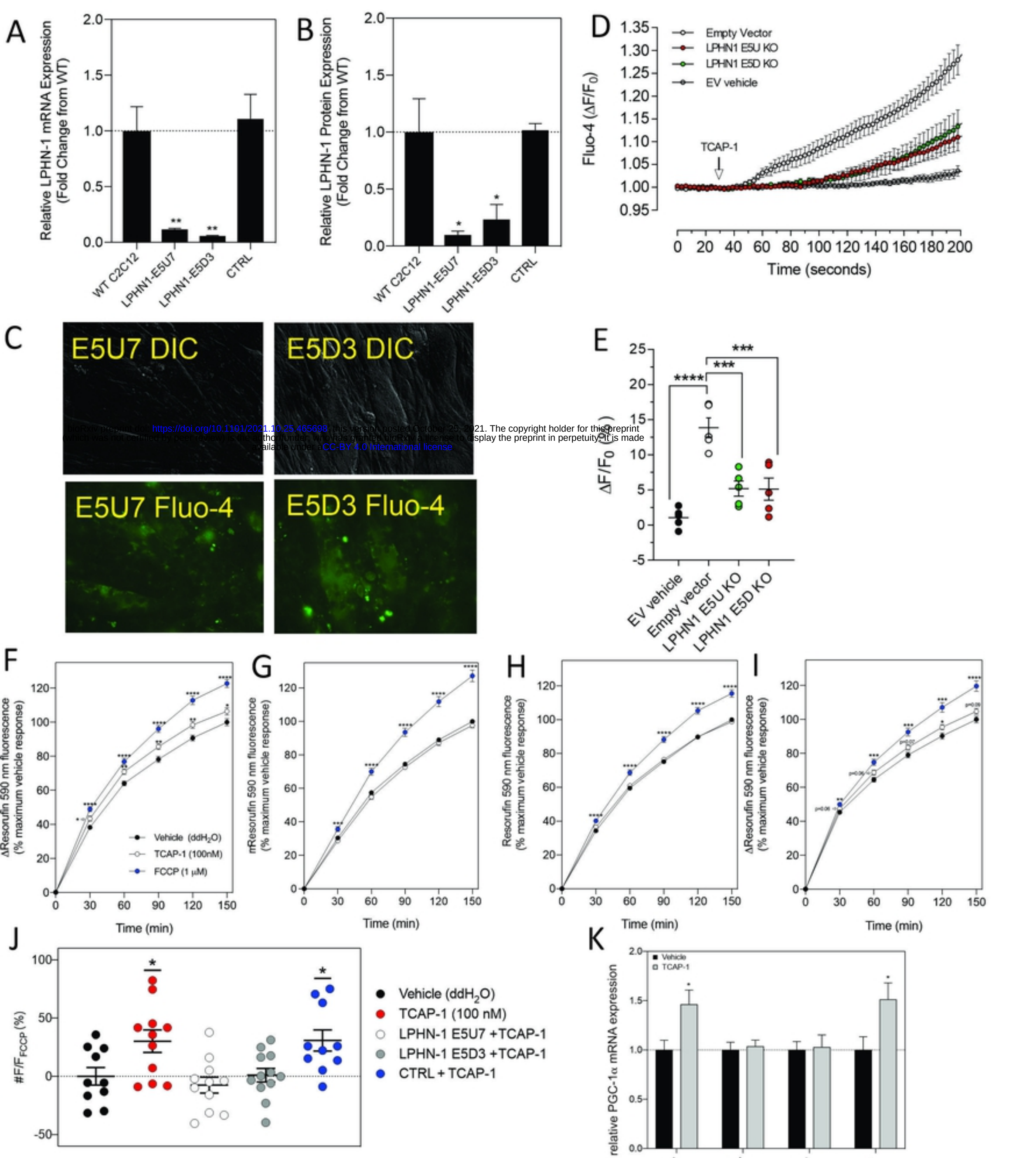

Figure 11